General Disclaimer

One or more of the Following Statements may affect this Document

- This document has been reproduced from the best copy furnished by the organizational source. It is being released in the interest of making available as much information as possible.

- This document may contain data, which exceeds the sheet parameters. It was furnished in this condition by the organizational source and is the best copy available.

- This document may contain tone-on-tone or color graphs, charts and/or pictures, which have been reproduced in black and white.

- This document is paginated as submitted by the original source.

- Portions of this document are not fully legible due to the historical nature of some of the material. However, it is the best reproduction available from the original submission.

AFOSR Scientific Report
OSR 68-1666

Contract No. AF 49(638)-1623
Project No. 9781-01

68-20

THE THREE-DIMENSIONAL WAKE

BEHIND AN OBSTACLE ON A FLAT PLATE

by

Robert F. Mons and Pasquale M. Sforza

JUNE 1968

POLYTECHNIC INSTITUTE OF BROOKLYN

DEPARTMENT
of
AEROSPACE ENGINEERING
and
APPLIED MECHANICS

PIBAL REPORT NO. 68-20

OSR 68-1666

THE THREE-DIMENSIONAL WAKE BEHIND AN OBSTACLE ON A FLAT PLATE

by

Robert F. Mons and Pasquale M. Sforza

This research was supported by the Air Force Office of Scientific Research under Contract No. AF 49(638)-1623, Project No. 9781-01. Research monitored under the technical supervision of Major Donald L. Calvert, AFOSR.

POLYTECHNIC INSTITUTE OF BROOKLYN

Department

of

Aerospace Engineering and Applied Mechanics

June 1968

PIBAL Report No. 68-20

THE THREE-DIMENSIONAL WAKE BEHIND AN OBSTACLE ON A FLAT PLATE[†]

by

Robert F. Mons[*] and Pasquale M. Sforza[**]

Polytechnic Institute of Brooklyn

SUMMARY

An investigation of the three-dimensional, incompressible wake behind a blunt obstacle located at the leading edge of a flat plate is presented. Configurations studied included the "clean" flat plate, and the flat plate with a rectangular, a square, or a two-dimensional obstacle fitted to the leading edge of the plate. Experimental results are compared to a mathematical model based on the Oseen linearization for diffusive flows.

Based on mean flow measurements, a transition to turbulent flow was not encountered for any of the configurations examined. Such wakes are characterized by a region of strong vorticity immediately behind the obstacle followed by a region of viscous diffusion. Bulk properties of the wake-like flow and the applicability of the theoretical model were found to be highly dependent on the geometry of the obstacle.

---

† This research was supported by the Air Force Office of Scientific Research under Contract No. AF 49(638)-1623, Project No. 9781-01.

* NASA Fellow

** Assistant Professor of Aerospace Engineering

TABLE OF CONTENTS

Section		Page
I	Introduction	1
II	Theoretical Description Of Flow	4
III	Experimental Apparatus	8
IV	Results.	12
V	Conclusion	26
VI	References	27

LIST OF ILLUSTRATIONS

Figure		Page
1	Schematic Representation of Flow Field of Three-Dimensional Wall Wake.	30
2	Photo of Open Circuit Wind Tunnel.	31
3	Photo of Double Probe Sickle.	32
4	Photo of Flat Plate with Static Probes.	33
5	Details of Three-Dimensional Obstacles.	34
6	Growth of Displacement Thickness for Flat Plate Boundary Layer.	35
7	Decay of Maximum Velocity Defect.	36
8	Transverse Velocity Profiles for 1:1 Obstacle at $\overline{X}$ = 28.5.	37
9	Half-width Growth	38
10	Displacement Thickness for All Obstacles.	39
11	Flat Plate Boundary Layer Similarity Profiles.	40
12	Similarity Profiles for Two-Dimensional Obstacle.	41
13	Similarity Profiles for 10:1 Obstacle.	42
14	Similarity Profiles for 1:1 Obstacle.	43
15	Transverse Similarity Profiles for 10:1 Obstacle.	44
16	Transverse Profiles X = 0.50 in., Y = 0.010 in.	45
17	Transverse Profiles X = 0.50 in., Y = 0.050 in.	46
18	Transverse Profiles X = 1.00 in., Y = 0.010 in.	47
19	Transverse Profiles X = 1.00 in., Y = 0.050 in.	48
20	Non-Uniformity of Transverse Profiles for 1:1 Obstacle.	49
21	Normal Profile at X = 4.0 in. Compared to Linearized Theory.	50
22	Normal Profile at X = 5.0 in. Compared to Linearized Theory.	51
23	Normal Profile at X = 6.0 in. Compared to Linearized Theory.	52

Figure		Page
24	Normal Profile at X = 9.0 in. Compared to Linearized Theory.	53
25	Transverse Profile at X = 4.0 in. Compared to Linearized Theory.	54
26	Transverse Profile at X = 6.0 in. Compared to Linearized Theory.	55
27	Transverse Profile at X = 9.0 in. Compared to Linearized Theory.	56
28	Isometric for 10:1 Obstacle.	57
29	Isometric for 1:1 Obstacle.	58
30	Photo of Flow Field for 10:1 Obstacle Using Lampblack.	59
31	Photo of Flow Field for 1:1 Obstacle Using Lampblack.	60
32	Photo of Flow Field for 10:1 Obstacle Using Smoke.	61
33	Photo of Flow Field for 1:1 Obstacle Using Smoke.	62

LIST OF SYMBOLS

d = height of obstacle

L = width of obstacle

Re_d = Reynolds number based on length d

T = nondimensional streamwise coordinate

u = velocity

u_∞ = free stream velocity

X = streamwise coordinate

Y = normal coordinate

Z = transverse coordinate

$\bar{(\ )}$ = $(\ )/d$

α = $\frac{L}{2d}$

Δu = $u_\infty - u$

Δu^* = $u(x_o, y_o, z_o = 2.0 \text{ in.}) - u(x_o, y_o, z)$

τ = nondimensional normal coordinate

ν = kinematic viscosity

ξ = nondimensional transverse coordinate

τ = nondimensional streamwise coordinate

φ = $\frac{u}{u_\infty}$

Subscripts

max = maximum value at a particular X coordinate

1/2 = denotes conditions at a station where $\Delta u = \Delta u_{max}/2$

I. INTRODUCTION

An investigation of the three-dimensional, incompressible wake behind a blunt obstacle located at the leading edge of a flat plate is presented. Results of experimental investigations utilizing the flat plate alone and the flat plate with two-dimensional, rectangular or square three-dimensional obstacles are compared to a theoretical investigation based on the Oseen linearization. This study constitutes one part of an extensive study of three-dimensional effects in fluid dynamics under investigation at the Polytechnic Institute of Brooklyn Aerospace Laboratories (PIBAL).

The occurrence of wakes behind obstacles on flat plates, which, for the purpose of this report, shall be called "wall wakes", is quite frequent. Fasteners protruding from the skin of airframes, spoilers, flaps, antenna masts, canopies, and land structures in a wind are just a few examples of configurations which can produce wall wakes. Furthermore, normal injection of a foreign gas from a wall into a uniform outer stream over the wall will produce a flow which is analogous in many respects to the flow produced by a blunt obstacle on a wall in a uniform flow.

A survey of the literature indicates relatively few investigations of the details of the entire flow field produced by configurations of the type examined in this report. Previous investigations have been primarily concerned with the effect of an obstacle on transition phenomena or on separation phenomena and have treated configurations wherein the obstacle is wholly or partially submerged in the boundary layer. Concerning transition, Tani[1] investigated two-dimensional and isolated roughness elements and presents a comprehensive bibliography on the subject. Klebanoff, Schubauer, and Tidstrom[2], Dryden[3], and Gregory and Walker[4], have performed similar investigations. Studies of the vortex distribution behind three-dimensional obstacles on a

flat plate have been performed by Hall[5] and by Weske[6], both of whom present excellent photographs and drawings of the flow field. Separation phenomena were examined by Peake, Galway, and Rainbird[7]. The effects of injection are examined by Torrence[8] and by Mickley and Davis[9]. Further experimental investigations are presented in References 10 - 12. Theoretical investigations have been performed by Eskinazi[11], Economos[13], and, for turbulent flows, by Abramovich[14]. Additional information is found in References 15 - 17.

The scope of the present study deviates markedly from that of the previously mentioned experimental investigations in that the location of the obstacle at the leading edge of the flat plate causes a large inviscid disturbance in the oncoming flow while the boundary layer forms downstream of this disturbance. Thus the purpose of this investigation is to examine the effects of large inviscid disturbances, caused by obstacles of various geometries, on a laminar boundary layer and, in so doing, to determine whether this type of flow can be adequately described by a simple analytical model, and to discover the existence of any significant departures from the expected diffusive behavior in flows of this type.

A schematic diagram of the flow field under investigation is shown in Figure 1. A uniform flow approaches a flat plate at zero degrees incidence. An obstacle standing normal to, and located at, the leading edge of the flat plate disturbs the oncoming flow and generates the wake-like flow. This wake behind a three-dimensional obstacle on a flat plate is found to be characterized by two distinct regions, namely:

1) Recirculation (trapped vortex) Region: In this region, the effects of the vorticity induced by the obstacle dominate over the effects of viscous diffusion. The velocity profiles are characterized by zero or slightly negative velocities (back flow) directly behind the obstacle changing to considerably greater than free stream

velocity at heights above the top edge of the obstacle, and

2) Viscous Diffusion Region: In this region, the effects of viscosity become predominant. The strong induced vortex diffuses and the velocity profiles are characterized by the commonly expected velocity defects. This region can be divided into two subregions, namely:

a) Characteristic Decay Region: In this subregion mixing effects due to the obstacle permeate the flow field; the flow is highly sensitive to obstacle geometry here.

b) Asymptotic Decay Region: In this subregion, viscous effects dominate the flow field and the flow asymptotes to the undisturbed boundary layer, i.e., the boundary layer becomes oblivious of the initial perturbation.

These regions are similar to those described by Trentacoste and Sforza[18] for free jets and by Viets and Sforza[19] and Sforza and Herbst[20] for wall jets.

In the theory developed for this flow no attempt has been made to describe the vortex distribution; rather, the mathematical model describes the region of viscous diffusion further downstream.

Results suggest that an obstacle located at the leading edge of a flat plate will not cause transition of the boundary layer on the plate for the conditions reported here.

II. THEORETICAL DESCRIPTION OF FLOW

A mathematical model for the flow was formulated following closely the method outlined in Ref. (13) which superimposes a three-dimensional linearized diffusive flow over a two-dimensional linearized boundary layer flow. Laminar flow with constant fluid properties is assumed.

In the absence of streamwise pressure gradients, the boundary layer equation describing the diffusion of a three-dimensional disturbance has the form:

$$(q\cdot\nabla)\varphi = \nu\nabla_1^2\varphi \qquad (1)$$

where $\varphi = \frac{u}{u_\infty}$ a non-dimensional velocity, $q\cdot\nabla$ is the usual three-dimensional convective operator, and $\nabla_1^2 \equiv \frac{\partial^2}{\partial y^2} + \frac{\partial^2}{\partial z^2}$. The kinematic viscosity, ν, is assumed to be constant.

Using the Oseen linearization, $q\cdot\nabla$ is replaced by $u_\infty \frac{\partial}{\partial x}$ (for $q = (u_\infty, o, o)$ this is exact). Equation (1) becomes

$$\frac{\partial\varphi}{\partial x} = \frac{\nu}{u_\infty}\nabla_1^2\varphi = \frac{d}{Re_d}\nabla_1^2\varphi \qquad (2)$$

where d is a characteristic length, and Re_d is the Reynolds number based on length d. The coordinates are now non-dimensionalized by the following transformations:

$$\tau = \frac{x-x_o}{d} = \bar{x}-\bar{x}_o,$$

$$\eta = \frac{y}{d}(Re_d)^{\frac{1}{2}} = \bar{y}(Re_d)^{\frac{1}{2}},$$

and

$$\tau = \frac{z}{d} (Re_d)^{1/2} = \bar{z} (Re_d)^{1/2},$$

where x_o is the position of the initial disturbance. Upon substitution, Equation (2) becomes

$$\frac{\partial \varphi}{\partial \tau} = \frac{\partial^2 \varphi}{\partial \eta^2} + \frac{\partial^2 \varphi}{\partial \xi^2} \cdot \qquad (3)$$

For the case of an obstacle of height d and width 2αd located at X = 0, the boundary conditions are:

$$\varphi(o, \eta, \xi) = \begin{cases} o : o \leq \eta \leq (Re_d)^{1/2}; |\xi| \leq \alpha (Re_d)^{1/2} \\ 1 : \text{otherwise} \end{cases},$$

$\varphi(\tau, o, \xi) = o$ (no slip at plate surface),

$\lim_{\eta \to \infty} \varphi(\tau, \eta, \xi) = 1$ $\quad (u \to u_\infty$ as $y \to \infty)$,

and

$\lim_{\substack{\tau \to \infty \\ \xi \to \pm \infty}} \varphi(\tau, \eta, \xi) = \varphi_1(\tau, \eta)$ (flow asymptotes to the linearized two-dimensional boundary layer flow).

The solution is separated into a two-dimensional uniform flow plus a three-dimensional disturbance. The two-dimensional uniform flow is described by the equatior

$$\frac{\partial \varphi_1}{\partial \tau} = \frac{\partial^2 \varphi_1}{\partial \eta^2} \cdot \qquad (4)$$

Boundary conditions are:

$$\varphi_1(\tau, o) = 0$$

and

$$\lim_{n \to \infty} \varphi_1(\tau, n) = 1 \qquad (u \to u_\infty \text{ as } y \to \infty).$$

The solution of this equation is

$$\varphi_1 = \operatorname{erf}\left(\frac{n}{2\sqrt{\tau}}\right) = \operatorname{erf}\left(\frac{\bar{y}}{2\sqrt{\bar{x}/Re_d}}\right),$$

where

$$\operatorname{erf}(x) = \frac{2}{\sqrt{\pi}} \int_o^x e^{-x'^2} dx'.$$

The three-dimensional disturbance is described by the equation

$$\frac{\partial \varphi_2}{\partial \tau} = \frac{\partial^2 \varphi_2}{\partial n^2} + \frac{\partial^2 \varphi_2}{\partial \xi^2} \quad . \tag{5}$$

The auxiliary conditions are:

$$\varphi_2(o, n, \xi) = \begin{cases} -1: & o \le \eta \le (Re_d)^{\frac{1}{2}};\ |\xi| \le \alpha \quad (Re_d)^{\frac{1}{2}} \\ 0: & \text{otherwise} \end{cases}$$

and

$$\lim_{\substack{\tau,\ n \to \infty \\ \xi \to \pm\infty}} \varphi_2(\tau, \eta, \xi) = 0.$$

The solution is, in general, given by

$$\varphi_2 = \tfrac{1}{4} \int_s \varphi_2\ (o, n, \xi)\ \frac{\partial F}{\partial \xi},\ \frac{\partial G}{\partial \eta},\ d\,\xi'\ d\,\eta', \tag{6}$$

where S is the surface on which the initial perturbation is described. Here

$$G(\tau, \eta; \eta') = \operatorname{erf}\left(\frac{\eta' - \eta}{2\sqrt{\tau}}\right) - \operatorname{erf}\left(\frac{\eta' + \eta}{2\sqrt{\tau}}\right)$$

and

$$F(\tau, \xi; \xi') = \operatorname{erf}\left(\frac{\xi' - \xi}{2\sqrt{\tau}}\right) .$$

Substituting the boundary condition yields

$$\varphi_2 = -1/4\left[\operatorname{erf}\left(\frac{1 - \bar{y}}{2\sqrt{\bar{x}/Re_d}}\right) - \operatorname{erf}\left(\frac{1 + \bar{y}}{2\sqrt{\bar{x}/Re_d}}\right) + 2\operatorname{erf}\left(\frac{\bar{y}}{2\sqrt{\bar{x}/Re_d}}\right)\right]\left[\operatorname{erf}\left(\frac{\alpha - \bar{z}}{2\sqrt{\bar{x}/Re_d}}\right) + \operatorname{erf}\left(\frac{\alpha + \bar{z}}{2\sqrt{\bar{x}/Re_d}}\right)\right] . \quad (7)$$

Let

$$T = \frac{\bar{x}}{Re_d}$$

and the velocity ratio

$$\varphi = \frac{u}{u_\infty} = \varphi_1 + \varphi_2 .$$

The final full solution for the wake-like flow far downstream is given by

$$\varphi = \operatorname{erf}\left(\frac{\bar{y}}{2\sqrt{T}}\right) - 1/4\left[\operatorname{erf}\left(\frac{1 - \bar{y}}{2\sqrt{T}}\right) - \operatorname{erf}\left(\frac{1 + \bar{y}}{2\sqrt{T}}\right) + 2\operatorname{erf}\left(\frac{\bar{y}}{2\sqrt{T}}\right)\right]\left[\operatorname{erf}\left(\frac{\alpha - \bar{z}}{2\sqrt{T}}\right) + \operatorname{erf}\left(\frac{\alpha + \bar{z}}{2\sqrt{T}}\right)\right] . \quad (8)$$

Results from the experimental investigation will be compared to this analytic result subsequently.

III. EXPERIMENTAL APPARATUS

1) Wind Tunnel

All experiments were performed in the seven-foot, subsonic, open-circuit wind tunnel located in the Propulsion Research Laboratory of the Polytechnic Institute of Brooklyn (refer to Figure 2). This tunnel is a commercially available unit manufactured by the Aerolab Supply Company, Hyattsville, Md. It features a twelve inch long by twelve inch diameter circular test section which is preceded by a contraction cone twenty-four inches long by twenty inches in diameter and is followed by a conical diffuser which is forty-eight inches long by twenty inches in diameter.

Power is provided by a constant speed A-C electric motor in direct drive with a fixed blade fan located at the exit. The intake and test sections are mounted as a single unit on a track. Airspeed is regulated by positioning the test section some fixed distance away from the exhaust section thereby admitting ambient air to the exhaust and thus bypassing the test section. This permits airspeeds of approximately ten to seventy-five feet/second in the test section. For uniformity of results, all experiments, except the low Reynolds number, flat plate boundary layer runs were performed with the wind tunnel completely closed.

Access to the test section is provided by a 3/4 in. wide by 8 in. long slot in the bottom of the test section. The probe was passed through this slot and the remainder of the slot was sealed to prevent stray sources of ambient air to the tunnel.

Temperature in the laboratory was maintained constant at $72^{\circ}F$, $\pm$ $2^{\circ}F$ at all times.

A calibration run was performed on the empty tunnel in the entire region where measurements were to be made. The results of this calibration showed that the velocity in this region is constant

to within approximately 3% with no steep gradients existing.

2) Probe and Pressure Measuring Equipment

A probe was designed to provide accurate positioning in three coordinate positions. The design permits six inches of streamwise movement (x coordinate), four inches of horizontal movement (z coordinate), and one and three-fourths inches of vertical movement (y coordinate). Accuracy of position was measured with a dial indicator and found to be $\pm$ 0.010 inches, $\pm$ 0.002 inches, and $\pm$ 0.003 inches respectively for the above positions. The probe tips were mounted on one of two "sickles", one of which is shown in Figure 3. One mounts either a static or a total pressure probe 0.018 inches in diameter; the other mounts both probes horizontally at a distance of 0.300 inches apart.

Pressure was measured on a manometer board inclined at 30^{o} to the horizontal; ethyl alcohol was used as manometer fluid. The tubes of the manometer have a relatively large inside diameter of one-fourth of an inch which, combined with the alcohol fluid, eliminates problems due to the fluid "wetting" the walls of the tubes. However, this size tube results in very slow response time when used with probes having inside diameters on the order of 0.006 inch. Because of this slow response, any fluctuations in the flow are effectively "integrated out" of the readings.

With the above manometer, pressure differences as low as 0.020 inches of alcohol are easily read. At the test velocities this corresponds to differences in velocity on the order of 0.5 to 1.0 feet/sec. Readings taken with the 0.018 inch probe tips were compared to readings taken with a standard N.P.L. roundnose pitot tube, one-eighth inch in diameter, and were found to differ by less than 0.020 inches alcohol at maximum velocity.

3) Test Plates

A number of flat plates were used during the course of the experiment. A typical plate appears in Figure 4. The two-dimensional plate is made of plexiglas with a removable leading edge made of aluminum. This leading edge was machined from bar stock to include a 0.100" x 0.050" obstacle across the entire leading edge. For the three-dimensional obstacles, a 1.000 inch wide by 1.250 inch long by 0.125 inch deep section was machined out of the leading edge. Inserts incorporating the various obstacles were machine out of aluminum and bolted to the plate. In all cases, bolts were located on the side of the plate opposite the test side. The obstacles used were 1.000 inch by 0.100 inch (10:1 obstacle) and 0.316 inch by 0.316 inch (1:1 obstacle), both with an area of 0.100 $\pm$ .005 square inches (refer to Figure 5). The thickness of the obstacles was 0.050 inches, thus boundary layer formation along the edge is negligible. For flat plate experiments a flat insert was used with the same plate used for three-dimensional experiments.

One plate was machined from plexiglas and incorporated a series of static orifices at the surface along the centerline. However, it was found that the plexiglas plate tended to "creep" or warp with time, thus causing irregularities in flatness. Therefore a plate with the same dimensions was machined from aluminum; however, the static orifices were not incorporated into the aluminum plate. This aluminum plate was used for all flat plate and three-dimensional experiments.

The plates were mounted in the tunnel so as to provide adjustment in the three coordinate planes. To establish trueness between the plate and the probe, a dial indicator was placed on the probe which was then moved transversely across the plate (z coordinate) and also along the plate centerline (x coordinate). This was done before and after testing, and in both cases variation was less than 0.005 inches,

said variation arising from a combination of irregularities in the probe movement and the plate flatness.

Centering of the probe was accomplished visually by lining up the probe tip with a line scribed down the centerline of the plate, this being done while the probe tip was in contact with the plate. This geometric center was checked against the aerodynamic center established by the velocity readings.

4) Flow Visualization

Two methods were used to visualize the flow over the plate. The first method was to coat the plate with a mixture of lampblack and kerosene and then initiate the flow over the plate. The mixture is sheared by the airflow, leaving an imprint of the flow field on the plate. The plate is then photographed after the kerosene has evaporated. Pictures of the flow field for the flat plate, the two-dimensional obstacle, and the 10:1 and 1:1 three dimensional obstacles were obtained by this method.

The second method used tobacco smoke injected through a special plate incorporating a small plenum chamber feeding a series of 1/16" diameter orifices along the centerline of the plate. Pictures of the flow field for the flat plate and the 10:1 and 1:1 three-dimensional obstacle were obtained by this method. In addition, obstacles of 1.000" x 0.100", 1.000" x 0.200", and 0.316" x 0.316" were placed on the plate at various X stations with two-sided tape to examine the effect of the location of the obstacle with respect to the leading edge. The various obstacles employed are shown in Figure 5.

Results from these visualizations will be discussed subsequently.

IV. RESULTS

1) Nature of the Base Flow

The base flow for this study consists of a uniform flow over a flat plate at zero angle of attack. The displacement thickness, δ^*, was numerically evaluated from the velocity profiles measured normal to the flat plate. Runs were made at Reynolds numbers of 4.10×10^4 per inch and 1.55×10^4 per inch, corresponding to free-stream velocities of 77 ft/sec and 29 ft/sec respectively. The displacement thickness is shown plotted as a function of X for both cases in Figure 6. For both cases the displacement thickness is relatively constant up to 3 in.; this is probably the result of leading edge effects. Beyond 3 in. the displacement thickness grows as $X^{0.44}$ at the higher velocity and as $X^{0.41}$ at the lower velocity. This rate of growth indicates a laminar boundary layer in both cases.

All subsequent wake studies were performed at a Reynolds number of 4.10×10^4 per inch; the low Reynolds number test mentioned previously was performed to confirm the existence of a laminar boundary layer. The existence of a laminar base flow is important because the application of the linearized theory, as presented in the previous section, is dependent upon specification of the transport property ν as a function at most of X alone. For laminar flow ν is a specified constant and the coordinate transformation may be handled with little difficulty.

2) Decay of Maximum Velocity Defect

The maximum velocity defect (Δu_{max}) at each X station is defined as the maximum difference between the actual velocity at the centerline in the wake region of an obstacle and the velocity that would exist if no obstacle were present. The maximum velocity defect was

determined by comparing the normal velocity profile at the center-line for each obstacle with the flat plate boundary layer profile at the same position. The non-dimensionalized maximum velocity defect $\frac{\Delta u_{max}}{u_\infty}$ is plotted as a function of $\bar{X}$ in Figure 7 for the two-dimensional obstacle and the 10:1 and 1:1 three-dimensional obstacles.

A discussion of the results obtained for the various obstacles appears below:

a) Two-Dimensional Obstacle: For the two-dimensional obstacle the maximum velocity defect is constant up to $\bar{X} = 5$. This region is termed the Recirculation (trapped vortex) Region due to evidence of back flow and strong standing vortices. In this region viscous dissipation effects are small compared to inertial effects.

From $\bar{X} = 5$ to $\bar{X} = 60$ the rate of decay of the maximum velocity defect is found to be $X^{-1.06}$. This second region is termed the Characteristic Decay Region because viscous effects have only partially penetrated the flow field, this penetration being highly dependent on the geometric configuration of the obstacle. In this region the effects of concentrated vorticity interact with viscous dissipation effects.

Beyond $\bar{X} = 60$ the rate of decay of the maximum velocity defect decreases; however, the indicated rate, $X^{-.40}$, is not necessarily accurate since it is determined by only two data points. Still it would appear that far downstream the rate of decay of the maximum velocity defect for the two-dimensional obstacle approaches the rate predicted by the linearized theory, namely $X^{-\frac{1}{2}}$. This last region is termed the Asymptotic Decay Region. In this region viscous effects dominate and the flow approaches the undisturbed boundary layer configuration.

b) 10:1 Obstacle: The decay of the maximum velocity defect for the 10:1 three-dimensional obstacle is similar to that for the two-dimensional obstacle mentioned above. Up to $\bar{X} = 10$ the maximum

velocity defect is constant; this again is the Recirculation (trapped vortex) Region.

From $\bar{X}$ = 10 to $\bar{X}$ = 40 the rate of decay is found to be $X^{-1.50}$; this is the Characteristic Decay Region.

Finally, beyond $\bar{X}$ = 40 the rate of decay is $X^{-.57}$ which again is reasonably close to the $X^{-\frac{1}{2}}$ rate predicted by the linearized theory. This last region is the Asymptotic Decay Region.

c) For the 1:1 obstacle, a markedly different behavior was observed for the maximum velocity defect. Similar to the other obstacles, the defect is initially constant, up to $\bar{X}$ = 4; however, beyond this distance the maximum velocity defect decays very rapidly and instead of a velocity defect a velocity excess was found to exist in the centerline of the wake region. The defect becomes indistinguishable beyond $\bar{X}$ = 20 while a velocity excess on the order of 6% of the free-stream velocity was clearly distinguishable even at $\bar{X}$ = 28.5, which was the farthest downstream position where measurements could be taken. The flow field in this region is found to be characterized by a large velocity excess in the center of the wake region, giving way to a small velocity defect far from the centerline and a return to the undisturbed boundary layer even farther from the centerline. This behavior can be seen in Figure 8 in which the non-dimensional velocity, $\frac{u}{u_\infty}$, is plotted as a function of $\bar{Z}$ for various values of $\bar{Y}$ at $\bar{X}$ = 28.5.

It is not clear what causes this velocity excess. One possibility is that the upward deflection of the flow caused by the obstacle causes high local acceleration of the flow above the obstacle which shows up as the velocity excess when the flow reattaches to the plate surface. Another possibility is that the boundary layer in the wake region becomes transitional, resulting in a turbulent-like boundary layer profile in this region. However, computation of the displacement thickness, δ^*, and the flow visualization, do not clearly distinguish the flow as laminar or turbulent in this region.

The flow field of the 10:1 obstacle also had slight excesses in the wake region far downstream, but these were very slight and were found only very close to the plate surface. The phenomenon warrants further investigation to establish its cause.

3) Wake Spreading: Velocity Halfwidths and Displacement Thickness.

The spreading of the wake downstream was measured in two ways: by the velocity halfwidths and by the displacement thickness.

The velocity halfwidth for a wake is defined as the value of the coordinate at which the velocity defect is one-half the maximum velocity defect. For the normal coordinate (y) the halfwidth is found by comparing the normal velocity profile at the centerline to the flat plate boundary layer profile at the same position. For the spanwise coordinate (z) the halfwidth is found from the transverse velocity profile at the height at which the maximum velocity defect occurs. These values are then non-dimensionalized by dividing by the height of the obstacle.

Because of the previously mentioned velocity excess in the flow field far downstream of the 1:1 obstacle, it is not clear whether a halfwidth can be defined for such a flow; therefore, halfwidths were computed only as far downstream as the defect existed.

Non-dimensional halfwidths for the two-dimensional and 10:1 and 1:1 three-dimensional obstacles are plotted as functions of $\overline{X}$ in Figure 9. For the 10:1 obstacle, the halfwidths cross at approximately $\overline{X} \approx 18$. This means that the wake is converging in the transverse direction while spreading in the normal direction in this region. This effect can be explained as a result of mass entrainment and vorticity. The Recirculation Region is a region of low static pressure which induces a mass flow into this region. In the spanwise direction there is no resistance to this induced flow while in the normal direction the flat plate blocks a normal flow. The net

result is a shrinking in the spanwise direction. This mass entrainment effect is strengthened by the strong vorticity induced by the obstacle. The effect of this vorticity is to induce a transverse velocity component towards the center of the wake. A similar argument holds for the 1:1 obstacle for which the halfwidths cross at $\overline{X} = 2.8$.

In the Asymptotic Decay Region the halfwidths for the two-dimensional and 10:1 obstacle grow at a rate close to the rate of $X^{\frac{1}{2}}$ predicted by the linearized theory. Because of the difficulty in defining the halfwidth for the 1:1 obstacle, it is not clear what the far downstream rate of growth is.

The displacement thickness, δ^*, was numerically calculated at the centerline for each of the configurations tested to compare this quantity to the halfwidth as a useful parameter for measuring growth of the wake. The displacement thickness, in inches, is plotted as a function of X in Figure 10 for the two-dimensional and 10:1 and 1:1 three-dimensional obstacles and for the flat plate boundary layer. It is noted that for each obstacle there is a large initial flow displacement followed by a region where the displacement thickness decreases such that it approaches the undisturbed boundary layer displacement. In particular, it is noted that for the 1:1 obstacle the displacement thickness is actually smaller than that of the flat plate boundary layer beyond X = 7.5 inches. This is a result of the previously mentioned velocity excess which appears in the centerline region of the wake of the 1:1 obstacle. It is to be expected that if measurements could have been taken further downstream, the displacement thickness for each obstacle would converge to the values for the undisturbed flat plate boundary layer indicating that the initial perturbation, due to the obstacle, has been obliterated by viscous dissipation and thus the flow is approaching a simple two-dimensional flat plate boundary layer flow.

It was hoped that the rate of growth of the displacement thickness far downstream would indicate whether the boundary layer remained laminar, but it was not possible to take measurements far enough downstream to clearly establish the rate of growth. The displacement thickness does not really give an indication of the spreading of the wake but rather it is a measure of streamline deflection which is a measure of boundary layer growth.

4) Profile Similarity

The flow fields for each of the configurations tested were examined for similarity of the velocity profiles. It should be noted that strict similarity does not exist in the linearized solution obtained in Section II; however, the similarity observed by Viets and Sforza[19] and by Sforza[20] and Herbst for turbulent wall jets and the fact that in the far wake region the flow is approaching an undisturbed boundary layer flow suggested that reasonable similarity might exist.

Similarity of the flat plate boundary layer profiles is shown in Figure 11. The velocity is non-dimensionalized by dividing by the free stream velocity and the normal coordinate is non-dimensionalized by dividing by the displacement thickness, δ^*. Excellent similarity is exhibited in the flat plate boundary layer profiles.

Figures 12, 13, and 14 show velocity profiles normal to the plate at Z = 0 for the two-dimensional and 10:1 and 1:1 three-dimensional obstacles. The profiles for each obstacle exhibit reasonably good similarity in these plots. At first it might appear that the similarity in the normal profiles is a result of the boundary layer like flow in the far wake region; however, despite the overall similarity to a flat plate boundary layer profile, the profiles for each obstacle are clearly distinct even nine inches downstream.

It has been found frequently that the halfwidth is an excellent

similarity parameter for flows involving mixing, i.e., wake-like and jet-like flows. However, in the present study, it is found that the displacement thickness, δ^*, is a more useful similarity parameter than the halfwidth for the normal velocity profile. This result is probably a consequence of the boundary layer like nature of the flow in the far wake region, that is, the momentum defect due to the obstacle in the far wake region is small compared to the momentum loss due to shear at the plate surface. For flows over a wall, it might be concluded that the normal halfwidth is the better similarity parameter when the perturbation fluid supplies most of the momentum difference in the flow, for example, in the case of injection over a wall into a quiescent ambient, while the displacement thickness is the better similarity parameter when the perturbation fluid supplies only a small fraction of the total momentum difference, which is the situation in the present study.

The transverse velocity profiles for the three-dimensional obstacles were also examined for similarity. As previously mentioned, the transverse profiles for the 1:1 obstacle were in sharp contrast to the commonly expected far wake profiles, which are generally characterized by a maximum velocity defect at the centerline with a gradual return to the undisturbed flow far from the centerline. Instead, the far wake profiles for the 1:1 obstacle are found to be characterized by a velocity excess at the centerline which changes gradually to a slight velocity defect at $\bar{Z} \approx 3$ with a very gradual return to the undisturbed velocity very far from the centerline ($\bar{Z} \approx 6.5$). Because of this behavior, it is not clear how to define any similarity parameter for the transverse velocity profiles for the 1:1 obstacle, nor is it clear how to non-dimensionalize the velocity for such a profile; hence, these profiles were not examined for similarity.

The transverse velocity profiles for the 10:1 obstacles are more amenable to similarity analysis since a maximum velocity defect is

clearly definable in the far wake region of this obstacle. Figure 15 shows $\frac{\Delta u^*}{\Delta u^*_{max}}$ plotted as a function of $Z/Z_{\frac{1}{2}}$ at $Y = Y_{max}$ for various X stations. Here Δu^* is the difference between the undisturbed boundary layer velocity (at Z = 2.0 in.) at the given X and Y coordinates and the local velocity at a given value of Z. $Z_{\frac{1}{2}}$ is the value of the Z coordinate where $\Delta u^* = \frac{\Delta u^*_{max}}{2}$. It is found that the transverse velocity profiles for this obstacle exhibit reasonably good similarity. Note that the above described non-dimensionalization transforms a wake-like profile into a jet-like profile, hence the usefulness of the half-width as the similarity parameter.

5) Non-Uniformities in the Flow Field

Two types of non-uniformities were found to exist in the flow-field of the three-dimensional obstacles. One is a large velocity excess occurring at the coordinates corresponding to the edges of the obstacles in the near wake region; the other is a velocity excess occurring at the centerline of the wake in the far wake region of the 1:1 obstacle primarily. The first type of irregularity is shown in Figures 16, 17, 18, and 19 in which the velocity, non-dimensionalized by dividing by the free stream velocity is plotted as a function of Z for the flat plate, the two-dimensional obstacle, and the 10:1 and 1:1 three-dimensional obstacles. For both the flat plate and the two-dimensional obstacle the profiles are straight, indicating that these flows are indeed two-dimensional in nature. For both the 10:1 and 1:1 three-dimensional obstacles, the velocity directly behind the obstacle is zero, or slightly negative, indicating a recirculation region which is the Trapped Vortex Region. Beyond the edges of the obstacle, the velocity changes abruptly to greater than free stream velocity, this excess being as large as 20% of the free stream velocity. This behavior indicates the existence of a strong vortex region directly behind the obstacle, resulting in a severe velocity gradient at the coordinate corresponding to the edges of the obstacle. Further

evidence of vorticity is a slight decrease in static pressure at the same coordinates at which the non-uniformities occur. Beyond X = 2.0 inches there is no further evidence of strong vorticity, indicating that the induced vortices have been vitiated by the diffusive effects of the mixing process.

Irregularities of the type described above have been found by Torrence[9] for the case of normal injection of a foreign gas from a wall into a uniform supersonic flow over the wall. In this case, the irregularities were in the transverse concentration and Mach number profiles. The irregularities are pronounced at X/D = 15 but are non-existent at X/D = 30, which is approximately the same distance at which the velocity irregularities cease to exist in the present study. At high subsonic speeds, the existence of such irregularities could cause local supersonic regions in the flow with attendant problems of shock induced separation.

Figure 20 shows the non-dimensional velocity $\frac{u}{u_\infty}$ plotted as a function of Z at various X stations downstream of the 1:1 obstacle. The large velocity defect behind the obstacle at X = 0.5 inches changes to a velocity excess at X = 3.0 inches downstream; furthermore, the excess in the centerline region is well defined even at X = 7.5 inches and beyond. For the 10:1 obstacle a very small excess was observed far downstream and very close to the surface of the flat plate. The cause of this excess is not clear. Possibly the flow is becoming transitional in the region behind the obstacle. Another possibility is that the flow is locally accelerated when it is diverted upward and around the obstacle; this accelerated flow then reattaches to the plate further downstream, giving rise to a velocity excess close to the plate surface. Smoke pictures seem to indicate that the flow behind the obstacles remains laminar even far downstream, but the results are not conclusive; thus the observed non-uniformity cannot, at present, be explained with certainty.

6) Experiment Compared to Theory

The linearized theory presented in Section II is applicable to problems involving a perturbation on a uniform flow over a flat plate. A perturbation implies a small deviation from this base flow; certainly an impermeable obstacle located at the leading edge of the flat plate will produce a very large disturbance on the flow. It is not expected that the linearized theory will predict the nature of the flow in the near wake region of the obstacle because of the existence of a large velocity defect, concentrated vorticity, and normal and transverse pressure gradients and velocity components in this region. However, the above mentioned quantities diffuse rapidly, thus leading to a perturbed base flow to which the theory is applicable. It has been mentioned that for the two-dimensional and 10:1 three-dimensional obstacles bulk properties such as the rate of decay of maximum velocity defect and the rate of half-width growth in the far downstream region are close to the rates predicted by the linearized theory.

Because the analytic solution is not applicable to the near wake region, the streamwise coordinate T in the theoretical solution had to be matched to a particular X coordinate downstream where the experimental profiles matched the theoretical profiles reasonably well. The maximum velocity defect was used as the criterion for matching. As previously mentioned, the rate of decay of the maximum velocity defect for the 10:1 obstacle beyond $\bar{X} = 40$ was close to the $X^{-\frac{1}{2}}$ rate predicted by the linearized theory; consequently, having found the value of T which corresponds to $\bar{X} = 40$, all subsequent values of T are directly proportional to the value of $\bar{X}$.

Normal velocity profiles for the two-dimensional and 10:1 three-dimensional obstacles are compared to normal velocity profiles predicted by the linearized theory for various X stations in Figures 21, 22, 23, and 24. The theoretical normal profile at Z = 0 for the 10:1 obstacle is the same as the theoretical normal profile for the

two-dimensional obstacle for values of T up to T = 4.0, which is the largest value used. The normal profiles exhibit poor matching for two reasons: first, the boundary layer profile from the linearized theory is greatly different from the measured boundary layer profiles; secondly, the flow has a large initial upward displacement due to the obstacle; hence, the obstacle influences the flow far above its own dimensions. The result is that the flow far downstream effectively "sees" a much larger obstacle at the leading edge. The displacement thickness for both the two-dimensional and 10:1 obstacles at $\overline{X} = 5$ is approximately twice the obstacle's height; hence, when specifying the boundary conditions for the linearized solution it might be reasonable to assume that the obstacle height is actually twice the real obstacle height.

Transverse velocity profiles for the 10:1 obstacles are compared to the theoretical transverse profiles in Figures 25, 26, and 27. In these figures, $\frac{\Delta u^*}{\Delta u^*_{max}}$ is plotted as a function of Z. The velocity defect Δu^* is used instead of u to eliminate the boundary layer influence on the profiles so that the velocity defect alone may be examined; this is done because of the poor matching of the normal profiles both at the centerline and at the undisturbed boundary layer (Z = 2.0 in.). These profiles exhibit only fair matching to the theoretical profiles. The basic shape of the profiles is similar, but the experimental profiles are considerably narrower than the predicted curves which is a result of the contraction of the wake in the transverse direction in the near wake region; this phenomena was discussed in Part 3 of this section.

Thus, for the 10:1 obstacle, it is found that the linearized theory, as formulated in Section II, predicts the rate of decay and the rate of spreading in the far wake region reasonably well, but it does not adequately describe the velocity profiles in any region. The reason for the poor prediction of the velocity profiles is be-

lieved to be the inadequacy of the description of the initial perturbation for the linearized solution. For ease of solution, a uniform defect over the area of the obstacle was assumed; however, it is found that, in reality, the initial disturbance is highly three-dimensional in nature. It was not expected that the linearized solution would adequately describe the near wake region, but it was hoped that it would provide a reasonably good model for the far wake region; however the flow in the far wake region is found to have a good "memory" of the highly three-dimensional upstream perturbation, thus leading to the inadequacy of the simple initial conditions.

For a somewhat better description of the far downstream flow behind a highly eccentric obstacle - such as the 10:1 - it seems reasonable to assume an obstacle height of 1.5 to 2 times the actual height, this to account for the initial large upward deflection of the flow, and to assume a width from .7 to .9 times the actual width, this to account for the contraction in the transverse direction in the near wake region. In addition, a more accurate description of the undisturbed flat plate boundary layer profile is needed. For a good description of the far downstream flow, one would probably have to use the experimental data at some particular downstream position to describe the initial conditions.

Since the primary purpose of the present study is to examine experimentally the basic behavior of the three-dimensional wall wake, and to attempt the use of a simple analytic model, the above described method of solution was not attempted.

The 1:1 obstacle produced a flow which could not be handled with the type of analysis previously presented. The existence of a velocity excess downstream is in opposition to what would normally be expected and precludes the use of the previously derived solution. As previously described for the 10:1 obstacle, one could use the experimental data to describe the initial conditions, but, for the same

reasons as for the 10:1 obstacle, this was not attempted.

7) Flow Visualization

To visualize the entire flow field, isometric representations of the data were constructed for the 10:1 and 1:1 three-dimensional obstacles. Velocity is non-dimensionalized by dividing by the free-stream velocity and is plotted along the X coordinate as a function of Y and Z in Figures 28 and 29. For clarity, Y is positive downward (the coordinate system with respect to the obstacles is shown in both of these figures). The previously mentioned properties, that is, the external flow, decay of velocity defect, the spreading of the wake, and the non-uniformities are discernable from these figures.

Figures 30 and 31 are photographs of the flows behind the 10:1 and 1:1 obstacles respectively, made with the lampblack solution. Both photographs clearly show the standing vortices at the edge of each obstacle, the recirculation region directly behind each obstacle (the dark region) and the return to an ordered streamwise flow further downstream.

Figures 32 and 33 are photographs of the flow behind the 10:1 and 1:1 obstacles respectively, made by smoke injection. It should be noted that there was difficulty in producing dense smoke pictures because of the velocity (75 ft/sec) and the large airflow (more than 3500 c.f.m.) in the tunnel. Such conditions require very large volumes of smoke. These photographs clearly show a region of reverse flow behind the obstacles, and the large upward displacement of the external flow caused by the obstacle. In addition, these photographs seem to indicate that the flow far downstream remains laminar.

Apparently, the region of nearly stagnant fluid behind the obstacle acts somewhat as a solid body and the main airflow is diverted around this region as if a solid streamline body were present, with the result that the flow reattaches and remains laminar. Previous

investigations indicate that at the test Reynolds number an obstacle in a laminar boundary layer, and having a height roughly equal to the displacement thickness of the boundary layer, will cause transition. However, these investigations examined the effect of an obstacle already in the boundary layer downstream from the leading edge, whereas the present investigation deals with an obstacle at the leading edge. In the former case, the obstacle is in a region of high shear while in the latter case the obstacle has a uniform flow impinging on it, and the boundary layer forms behind it; this may be a factor in the apparent stability of the boundary layer.

To try to confirm this idea, smoke pictures were taken of the flow over an obstacle at locations of 3, 6, and 9 inches from the leading edge; the obstacles used were 0.100 x 1.000 inches, 0.200 x 1.000 inches, and 0.316 x 0.316 inches (refer to Figure 5). These pictures seem to indicate some turbulence behind the obstacle, this turbulence increasing as the obstacle is larger or further downstream. These results are not conclusive and more detailed measurement, with an instrument such as the hot wire anemometer is needed.

V. CONCLUSION

An investigation of the flow properties of the three-dimensional incompressible wake behind an obstacle located at the leading edge of a flat plate has been presented. The important results may be listed as follows:

1) Based on mean flow measurements, a transition to turbulent flow was not encountered for any of the configurations examined. This result is contrary to the results of investigations where the obstacle is immersed in the boundary layer.

2) Wakes of this type are characterized by a region of strong vorticity immediately behind the obstacle followed by a region of viscous diffusion. Ultimately the large inviscid disturbance is obliterated by the dissipative effects of viscosity such that an ordinary two dimensional boundary layer is achieved. It is found that the maximum velocity defect is less than 10% of the free stream velocity at 90 obstacle heights downstream.

3) A mathematical model based on the Oseen linearization is found to adequately predict such bulk properties as the rate of decay of the velocity defect and the wake spreading only in the far wake and only for slender obstacles (width to height ratios of 10:1 or greater). This model is found to be inadequate for predicting velocity profiles if simple boundary conditions are employed in the formation of the model.

4) Large scale non-uniformities in the distribution of mean velocity were found in the three-dimensional flows, especially for a square obstacle. These non-uniformities could have important consequences in large scale applications.

The interaction between the strong vorticity field and the diffusive flow is believed to be the cause of the observed behavior in the near field of the flow, and areas for further investigation of this facet of the flow have been suggested.

VI. REFERENCES

1. Tani, I. "Effects of Two-Dimensional and Isolated Roughness on Laminar Flow", Boundary Layer and Flow Control, Vol. 2, Pergamon Press, 1961.
2. Klebanoff, P. S., Schubauer, G. B., and Tidstrom, K. D., "Measurements of the Effect of Two-Dimensional and Three-Dimensional Roughness Elements on Boundary Layer Transition", Journal of Aeronautical Sciences, 22, 1955.
3. Dryden, H. L., "Review of Published Data on the Effect of Roughness on Transition from Laminar to Turbulent Flow", Journal of Aeronautical Sciences, 20, 1953.
4. Gregory, N. and Walker, W. S., "The Effect on Transition of Isolated Surface Excrescences in the Boundary Layer", A.R.C. R & M No. 2779, 1956.
5. Hall, G. R., "Interaction of the Wake from Bluff Bodies with an Initially Laminar Boundary Layer", AIAA Paper No. 66-126, 1966.
6. Weske, J. R., "Experimental Study of Detail Phonomena of Transition in Boundary Layers", Institute of Fluid Dynamics and Applied Mathematics, University of Maryland, Tech. Note BN-91, February 1957.
7. Peake, D. J., Galway, R. D., and Rainbird, W. J., "The Three-Dimensional Separation of a Plane, Incompressible, Laminar Boundary Layer Produced by a Rankine Oval Mounted Normal to a Flat Plate", N.R.C. No. 8925, November 1965.
8. Torrance, M. G., "Concentration Measurements of an Injected Gas in a Supersonic Stream", NASA TN D-3860, April 1967.
9. Mickley, H. S. and Davis, R. S., "Momentum Transfer for Flow over a Flat Plate with Blowing", NACA TN-4017, November 1957.

10. Morduchow, M., Grape, R. G., and Shaw, R. P., "Stability of Laminar Boundary Layer near a Stagnation Point over an Impermeable Wall and a Wall Cooled by Normal Injection", NACA TN-4037, August 1957.
11. Eskinazi, S., "Mixing of Wakes in a Turbulent Shear Flow", NASA TN D-83, September 1959.
12. Klebanoff, P. S., "Characteristics of Turbulence in a Boundary Layer with Zero Pressure Gradient", NACA TN-3178, July 1954.
13. Economos, C., "Three-Dimensional Linearized Diffusive Flow with Arbitrary Initial Distribution", General Applied Science Laboratories, Inc., Technical Report No. 421, February 1964.
14. Abramovich, G. N., The Theory of Turbulent Jets, Chap. III, M.I.T. Press, Cambridge, Mass., 1963.
15. Steiger, M. H. and Bloom, M. H., "Three-Dimensional Effects in Viscous Wakes", Polytechnic Institute of Brooklyn, PIBAL Report No. 711, June 1962.
16. Schlichting, H., Boundary Layer Theory, McGraw-Hill Book Co., Inc., New York, 1960.
17. Goldstein, S., Modern Developments in Fluid Dynamics, Vols. I and II, Dover Publications, Inc., New York, 1965.
18. Trentacoste, N. and Sforza, P. M., "An Experimental Investigation of Three-Dimensional Free Mixing in Incompressible, Turbulent Free Jets", Polytechnic Institute of Brooklyn, PIBAL Report No. 871, AFOSR 66-0651, AD 634254, March 1966.
19. Viets, H. and Sforza, P. M., "An Experimental Investigation of a Turbulent, Incompressible, Three-Dimensional Wall Jet", Polytechnic Institute of Brooklyn, PIBAL Report No. 968, AFOSR 66-0888, AD 635010, April 1966.
20. Sforza, P. M. and Herbst, G., "A Study of Three-Dimensional, Incompressible, Turbulent Wall Jets", Polytechnic Institute of Brooklyn, PIBAL Report No. 1022, AFOSR 67-2580, AD 663423.

October 1967.

21. Schulze, W. M., Ashby, C. G., Jr., and Erwin, J. R., "Several Combination Probes for Surveying Static and Total Pressure and Flow Direction", NACA TN-2830, November 1952.

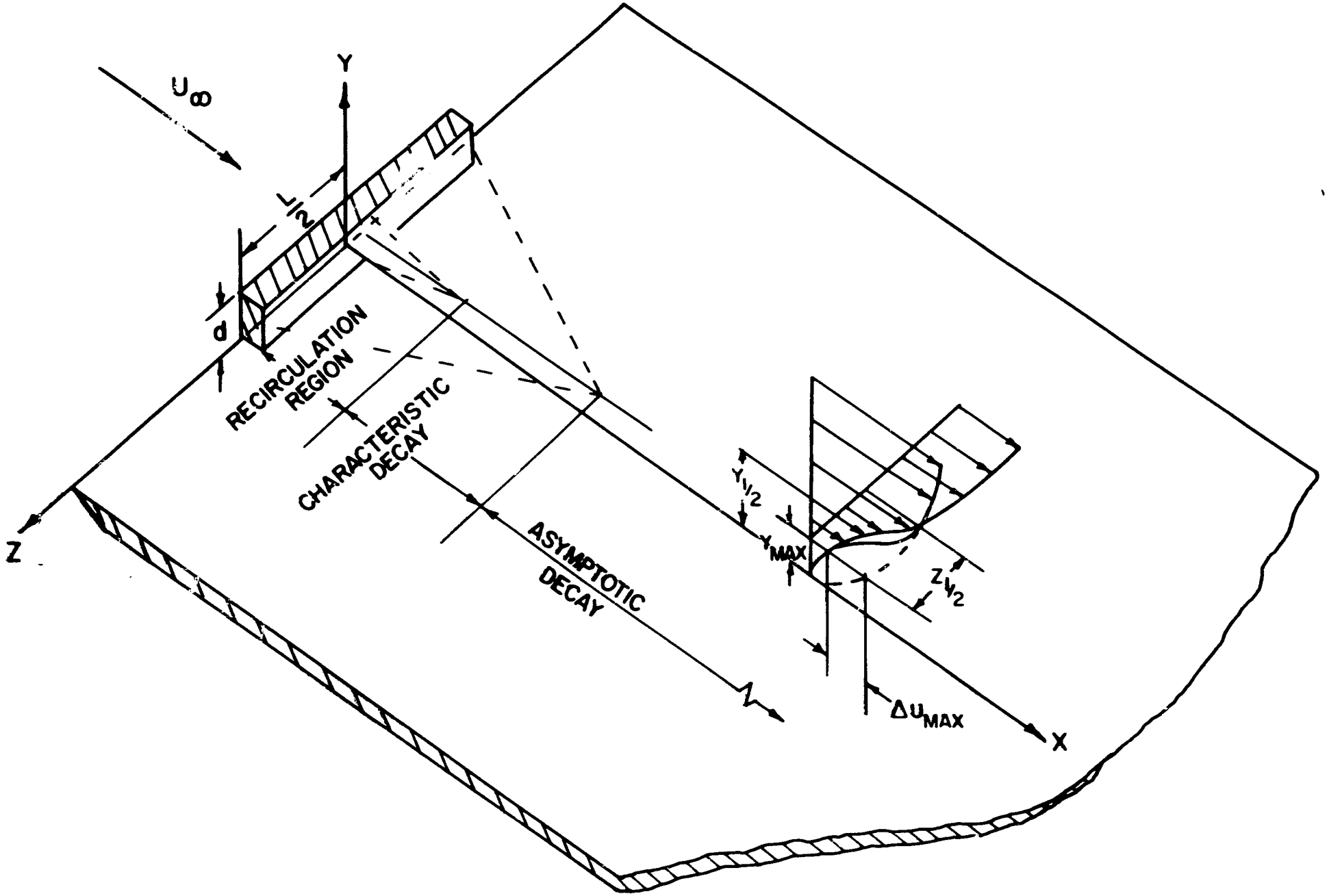

FIG. 1 SCHEMATIC REPRESENTATION OF FLOW FIELD OF THREE - DIMENSIONAL WALL WAKE

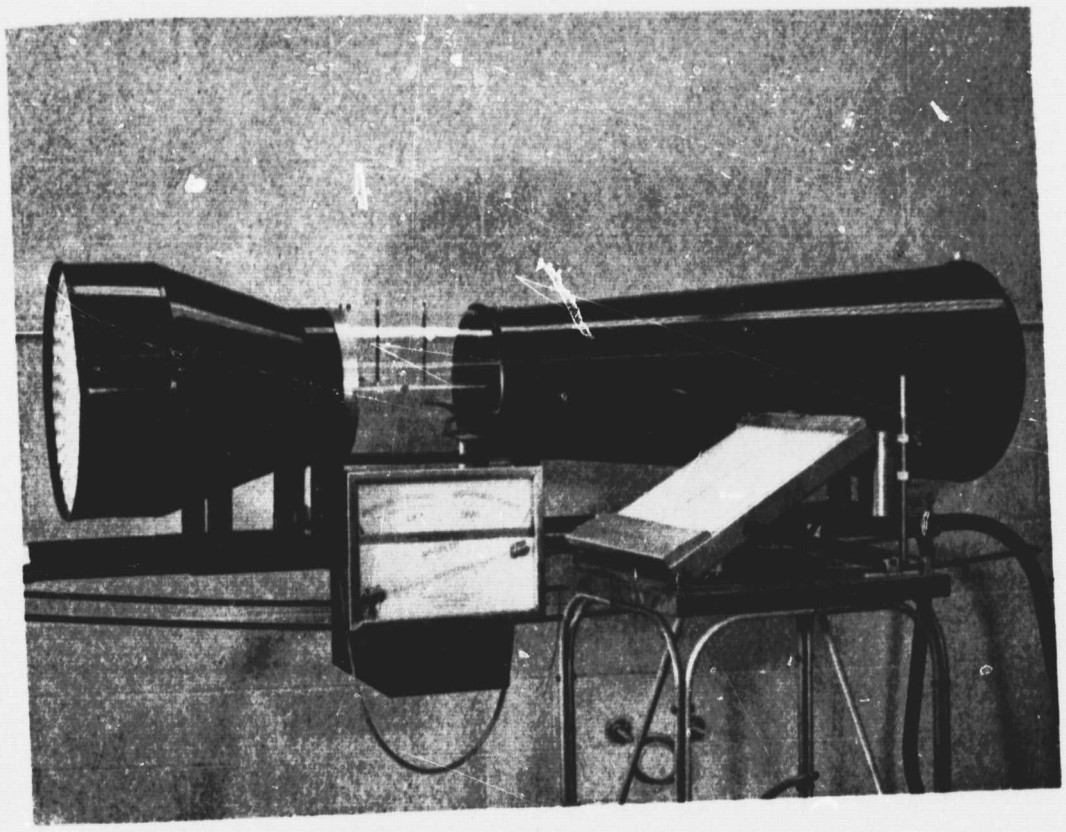

FIG. 2 PHOTO OF OPEN CIRCUIT WIND TUNNEL

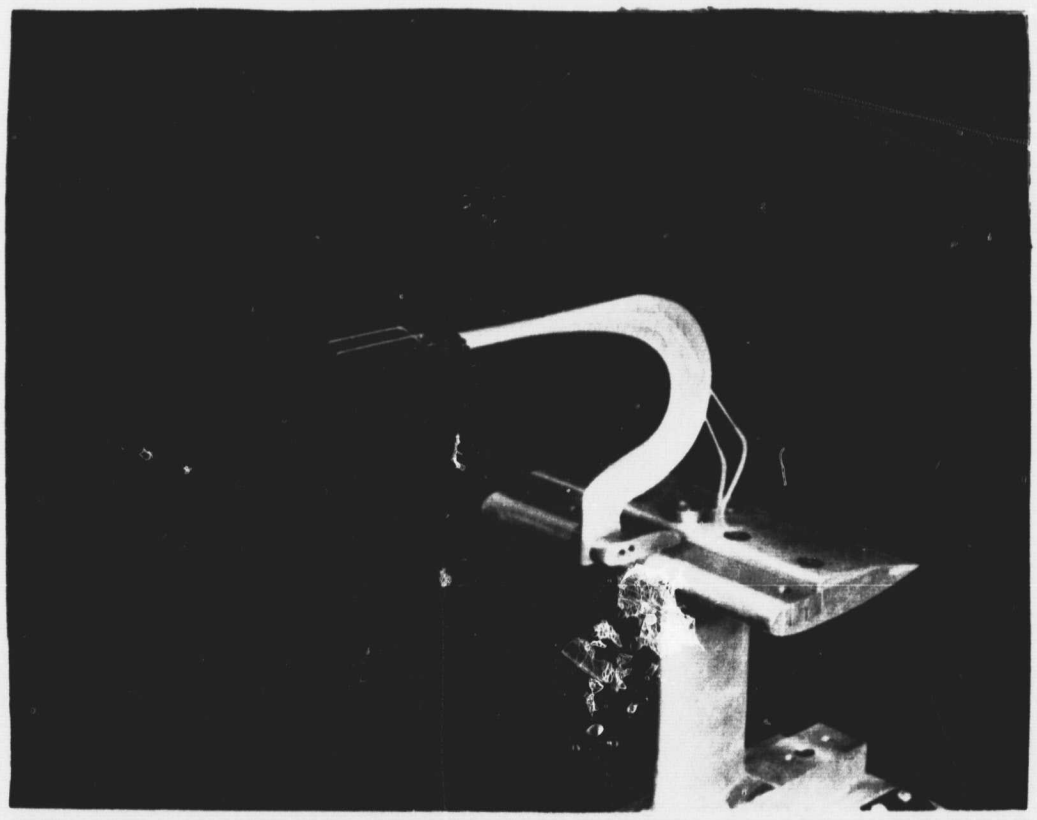

FIG. 3 PHOTO OF DOUBLE PROBE SICKLE

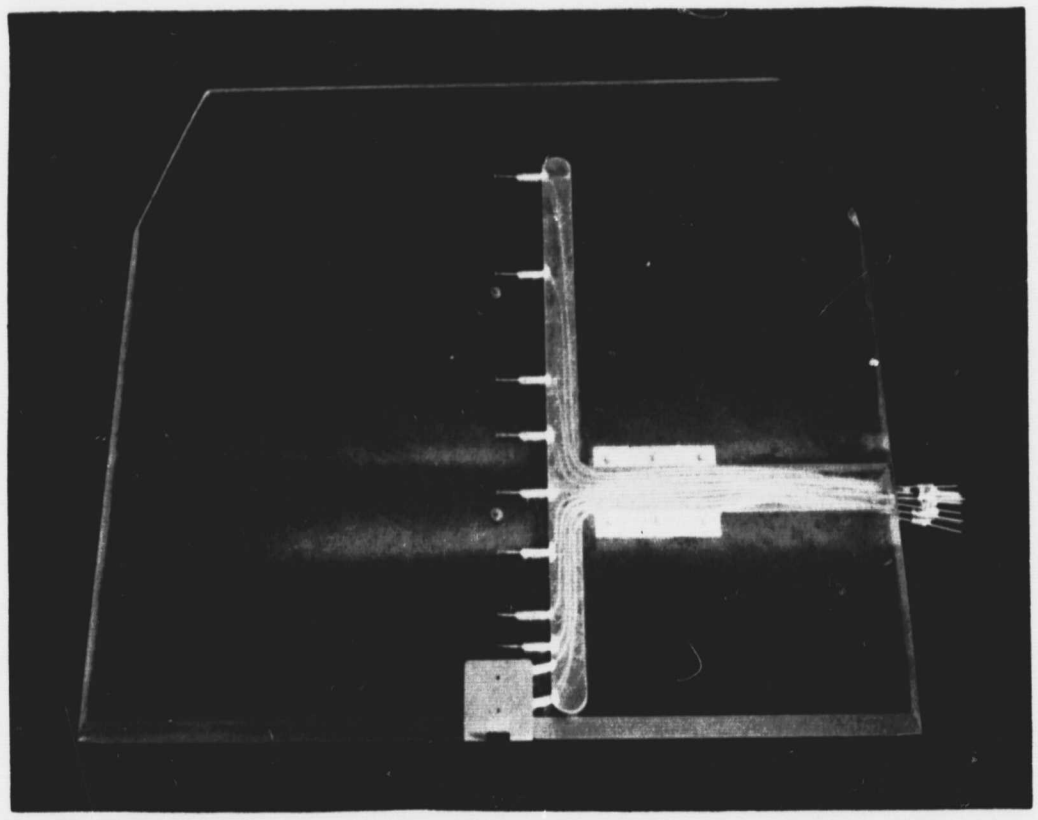

FIG. 4 PHOTO OF FLAT PLATE WITH STATIC PROBES

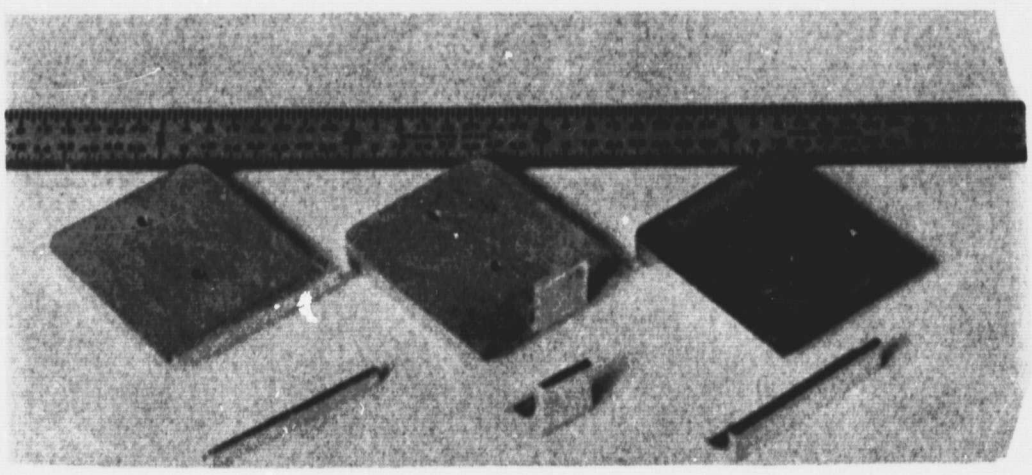

PHOTO OF OBSTACLES

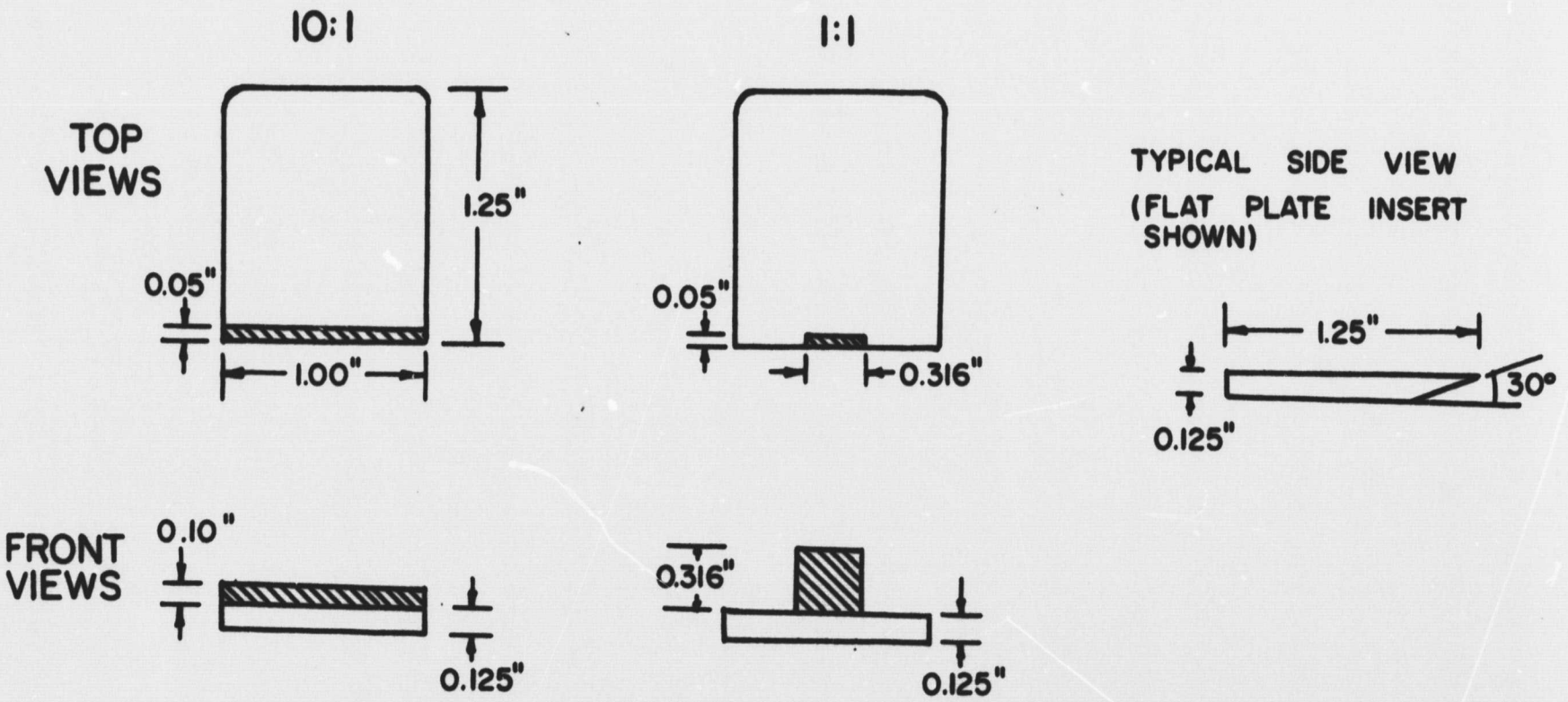

DIMENSIONS OF OBSTACLES

FIG. 5 DETAILS OF THREE-DIMENSIONAL OBSTACLES

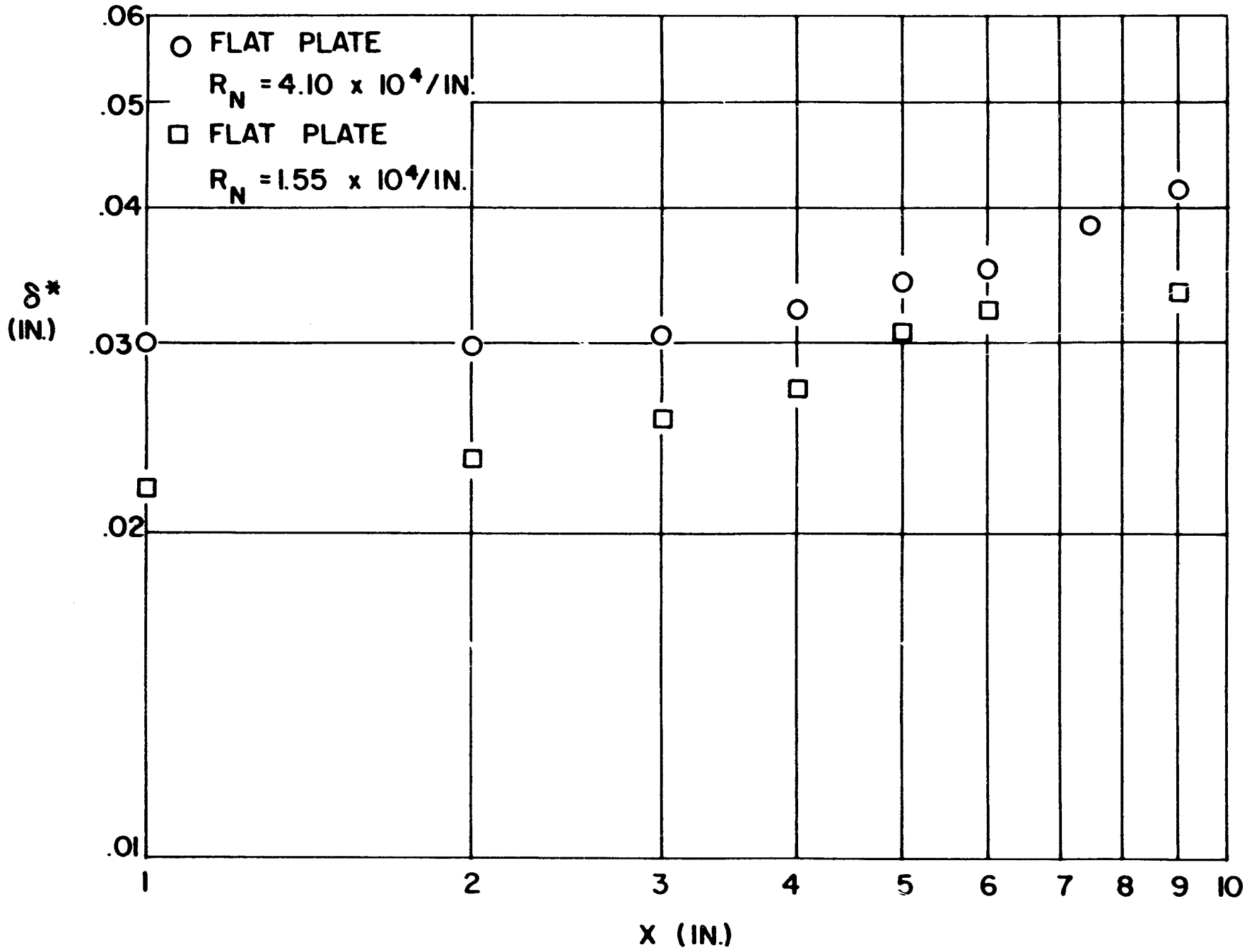

FIG. 6 GROWTH OF DISPLACEMENT THICKNESS FOR FLAT PLATE BOUNDARY LAYER

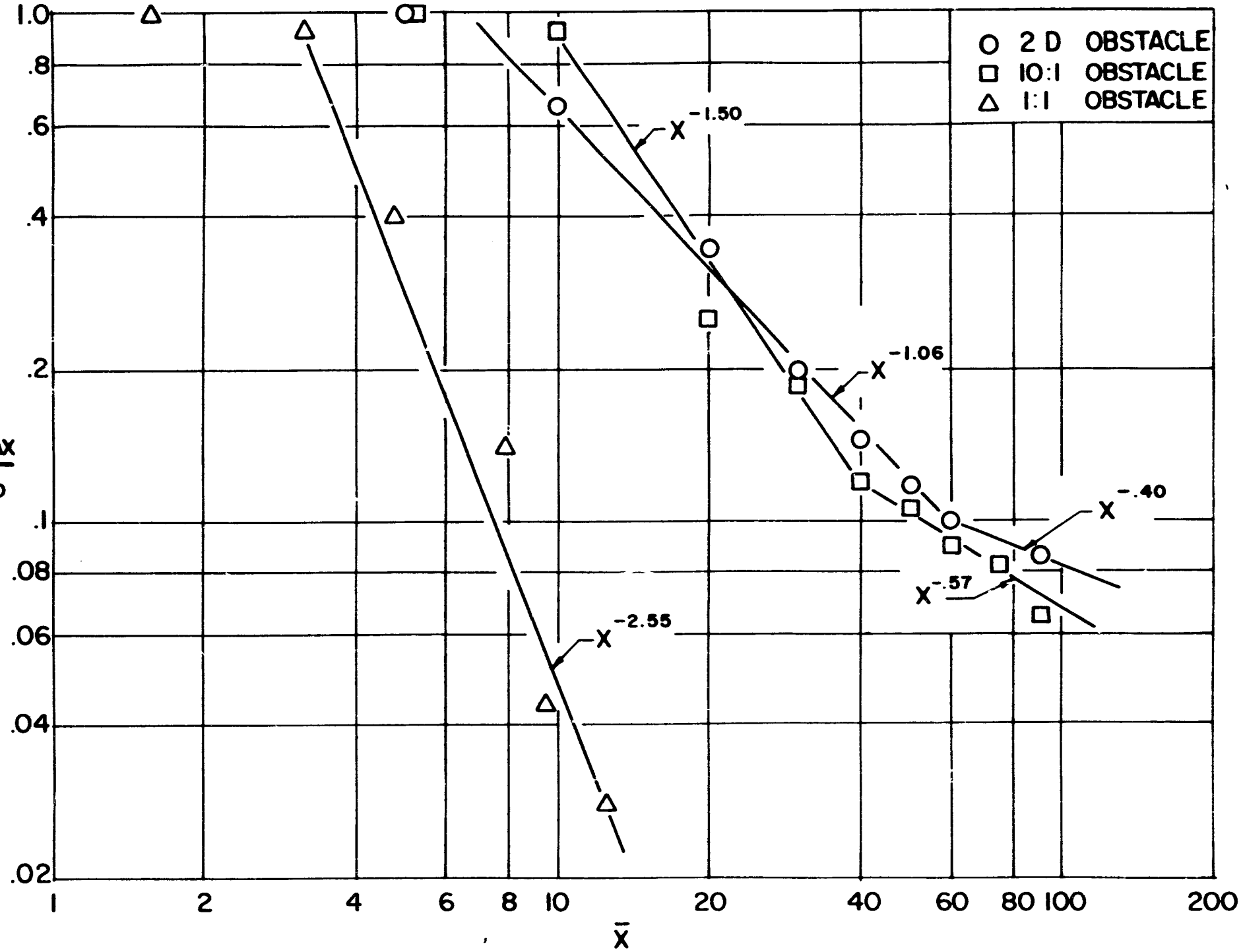

FIG. 7 DECAY OF MAXIMUM VELOCITY DEFECT

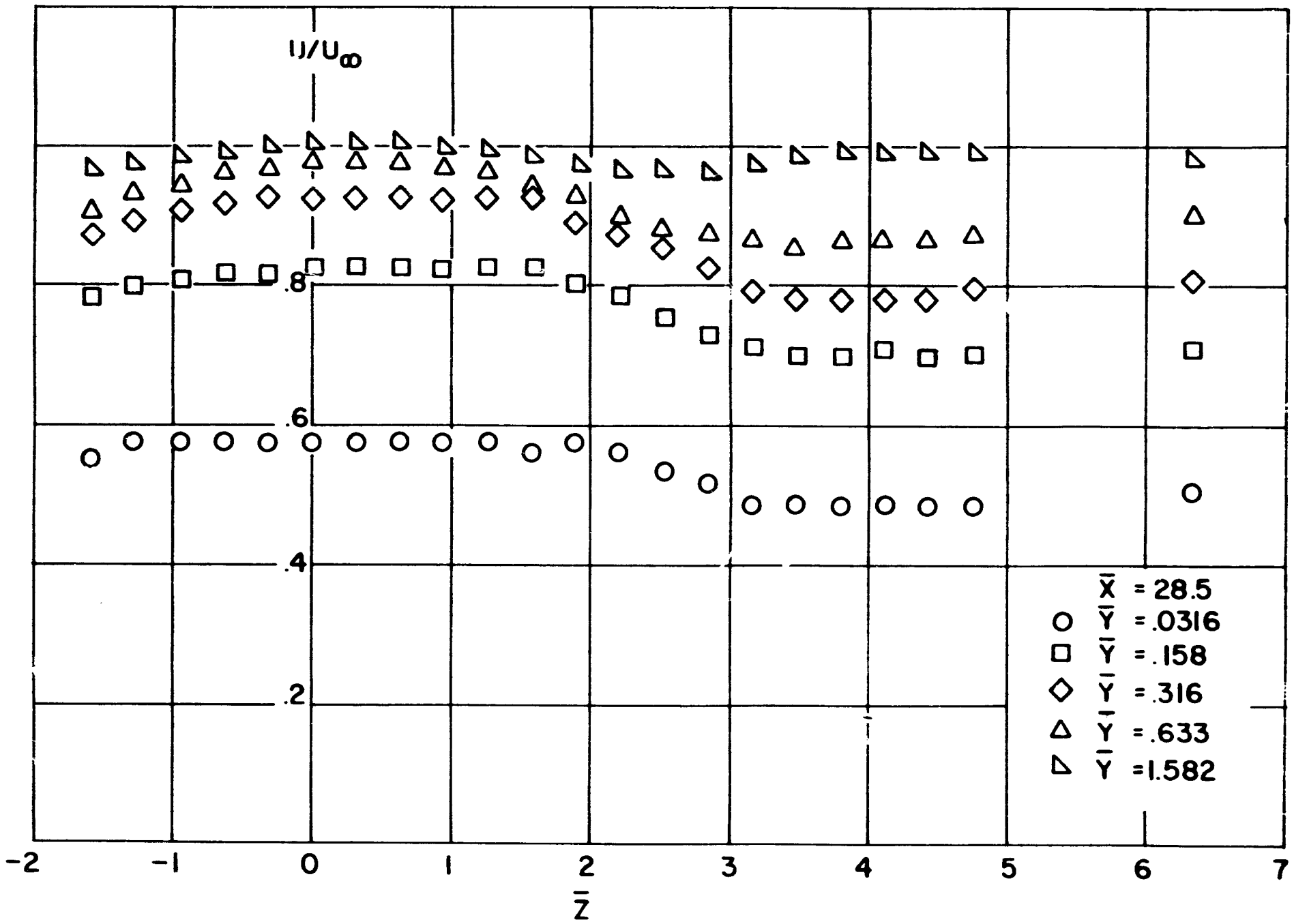

FIG. 8 TRANSVERSE VELOCITY PROFILES FOR 1:1 OBSTACLE AT $\bar{X} = 28.5$

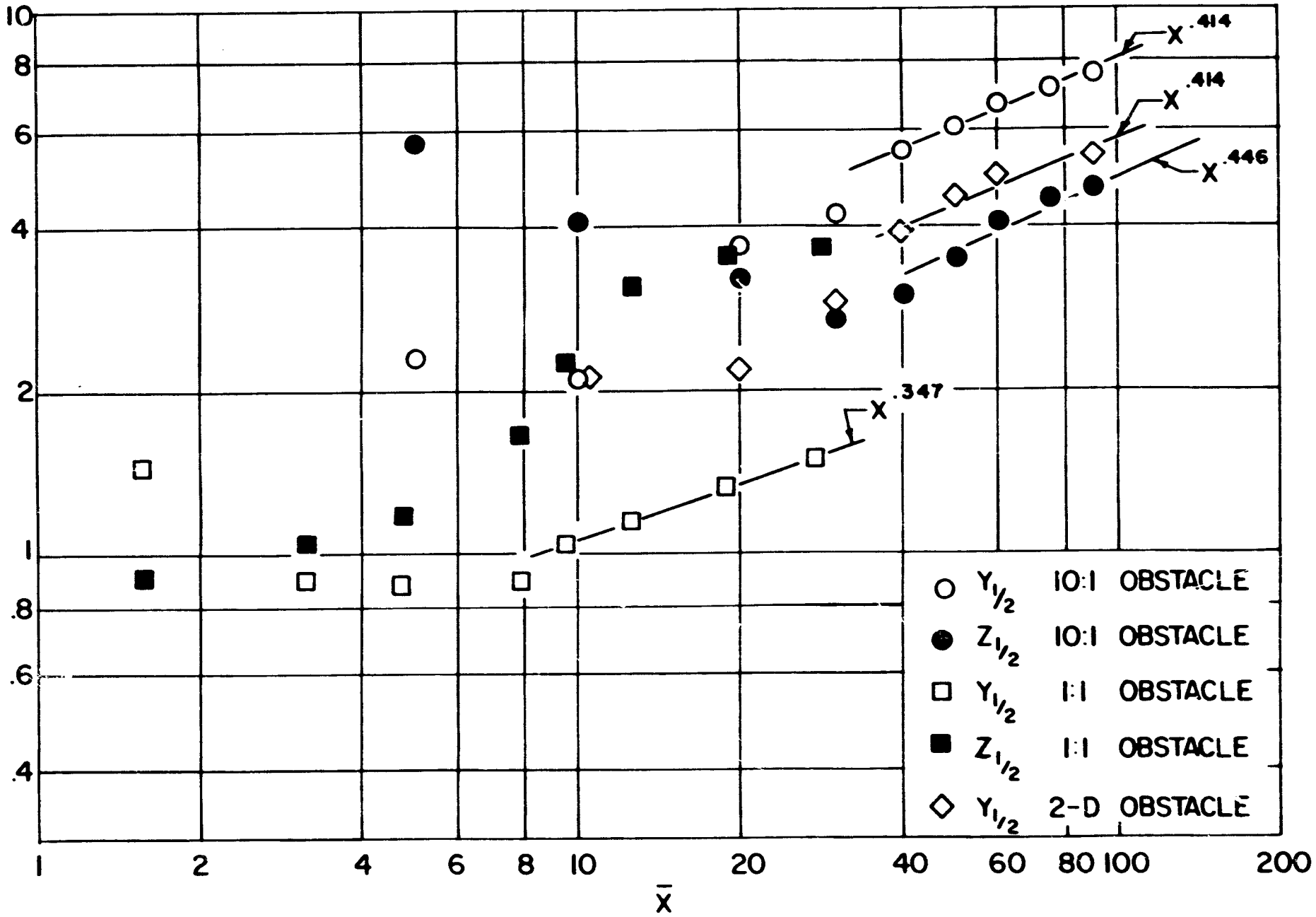

FIG. 9 HALFWIDTH GROWTH

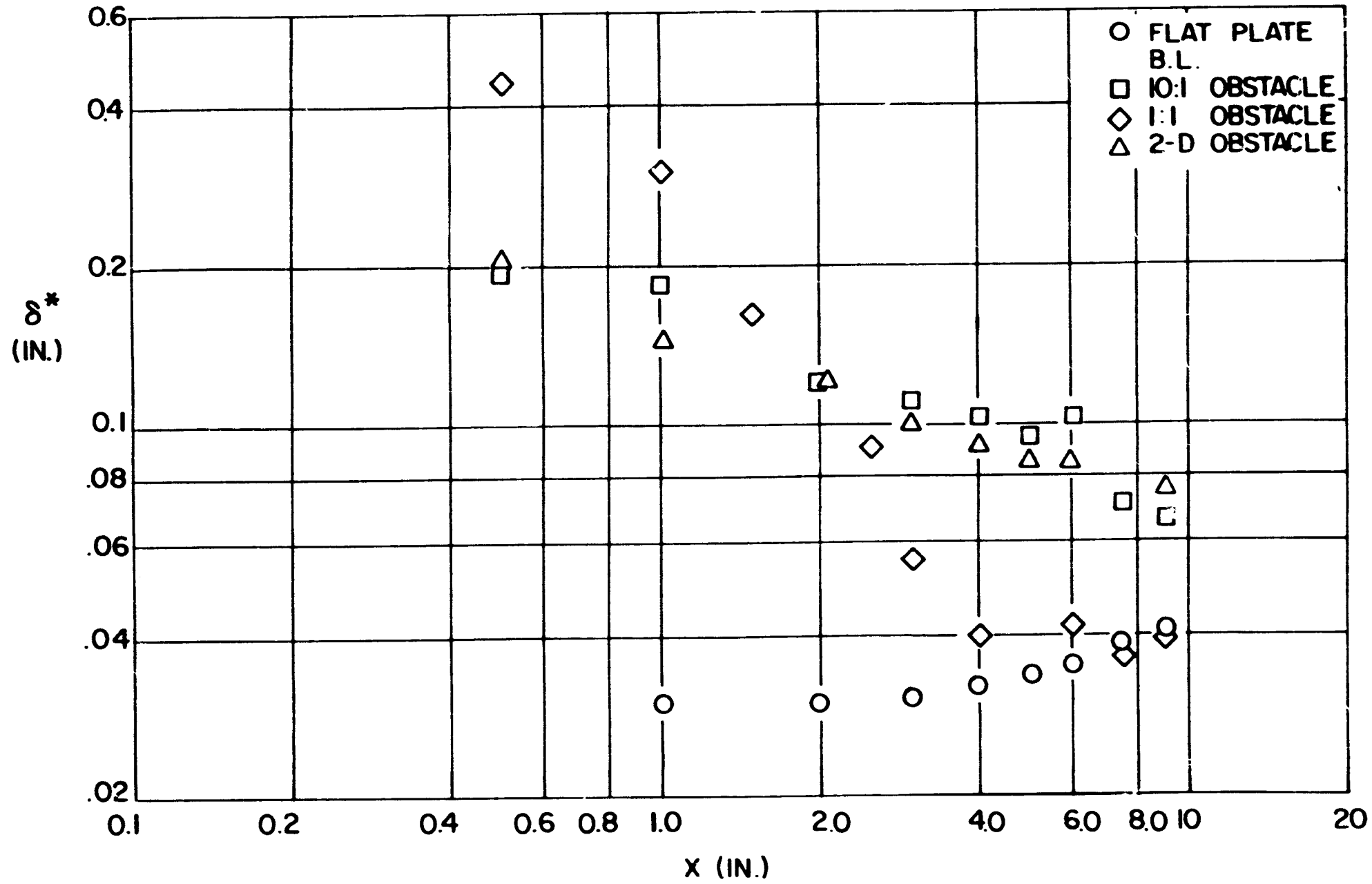

FIG. 10 DISPLACEMENT THICKNESS FOR ALL OBSTACLES

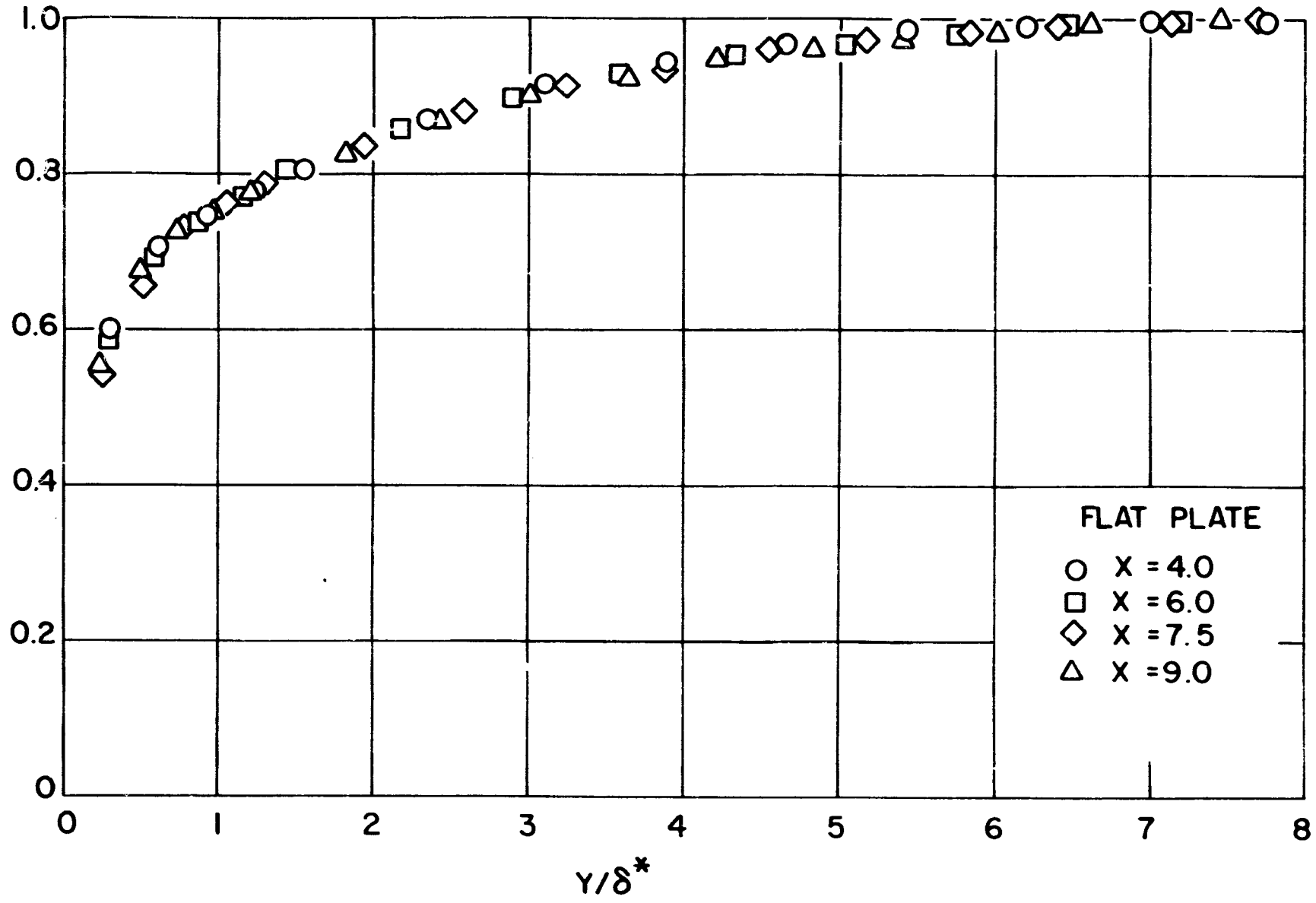

FIG. 11 FLAT PLATE BOUNDARY LAYER SIMILARITY PROFILES

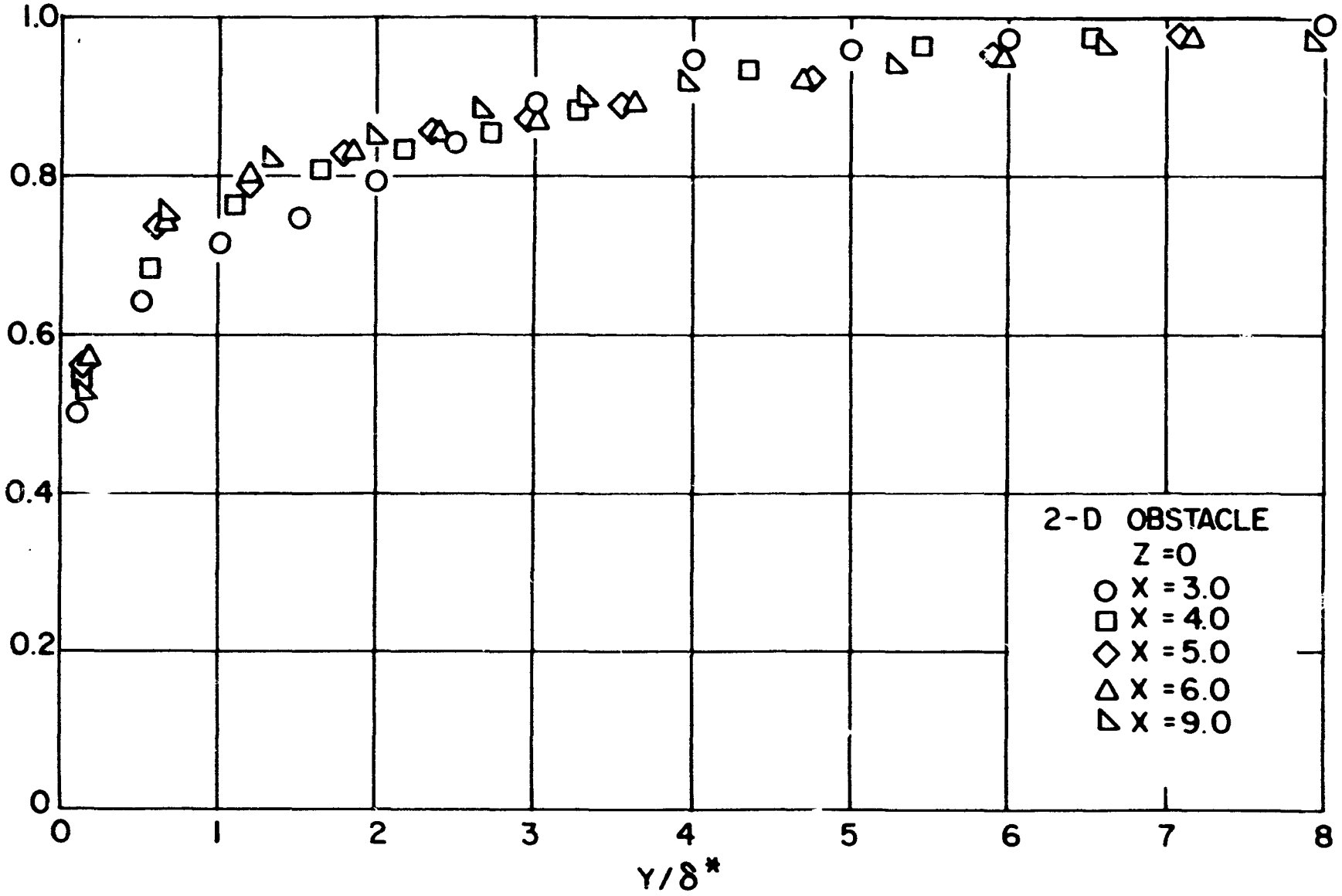

FIG. 12 SIMILARITY PROFILES FOR TWO-DIMENSIONAL OBSTACLE

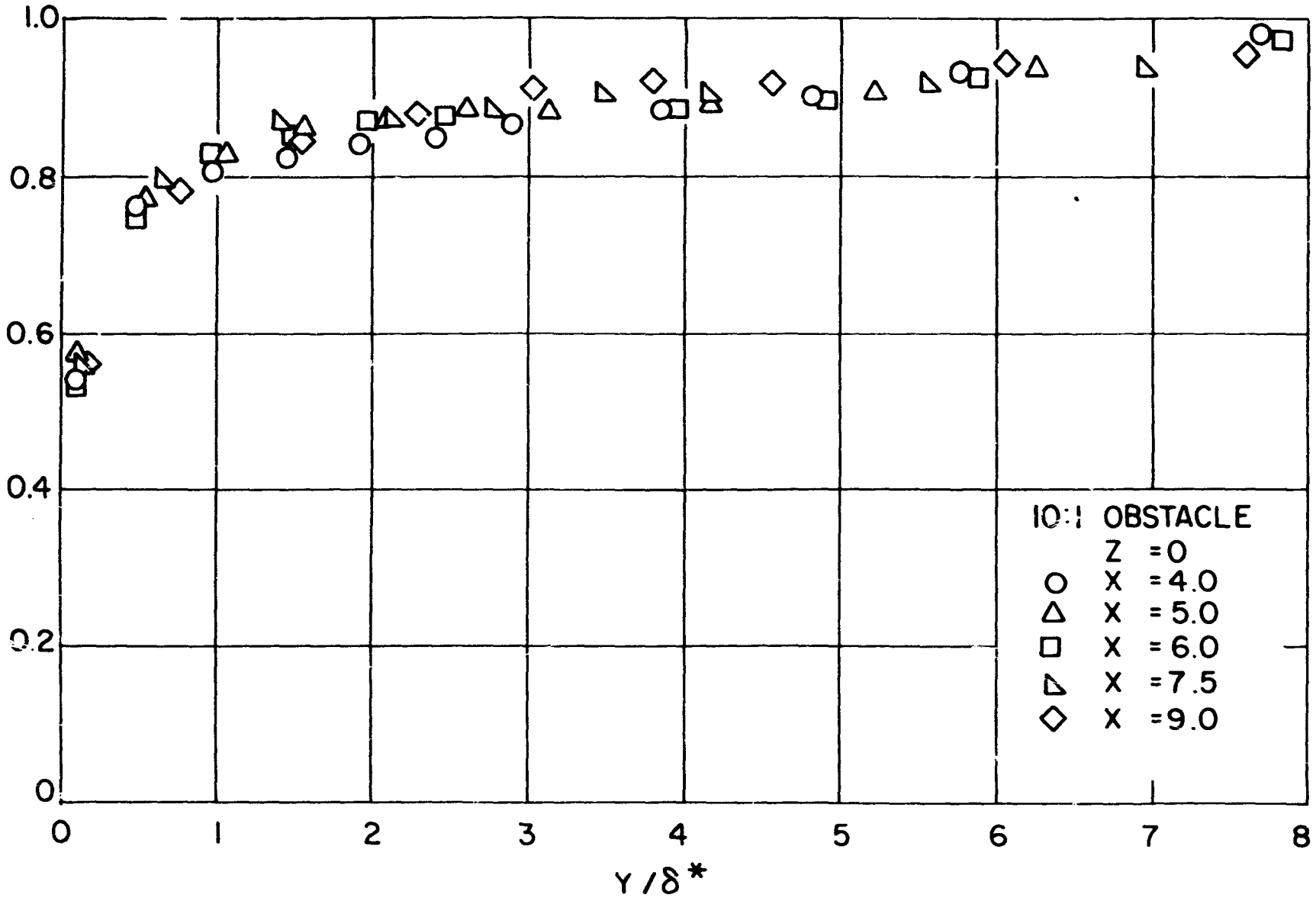

FIG. 13 SIMILARITY PROFILES FOR 10:1 OBSTACLE

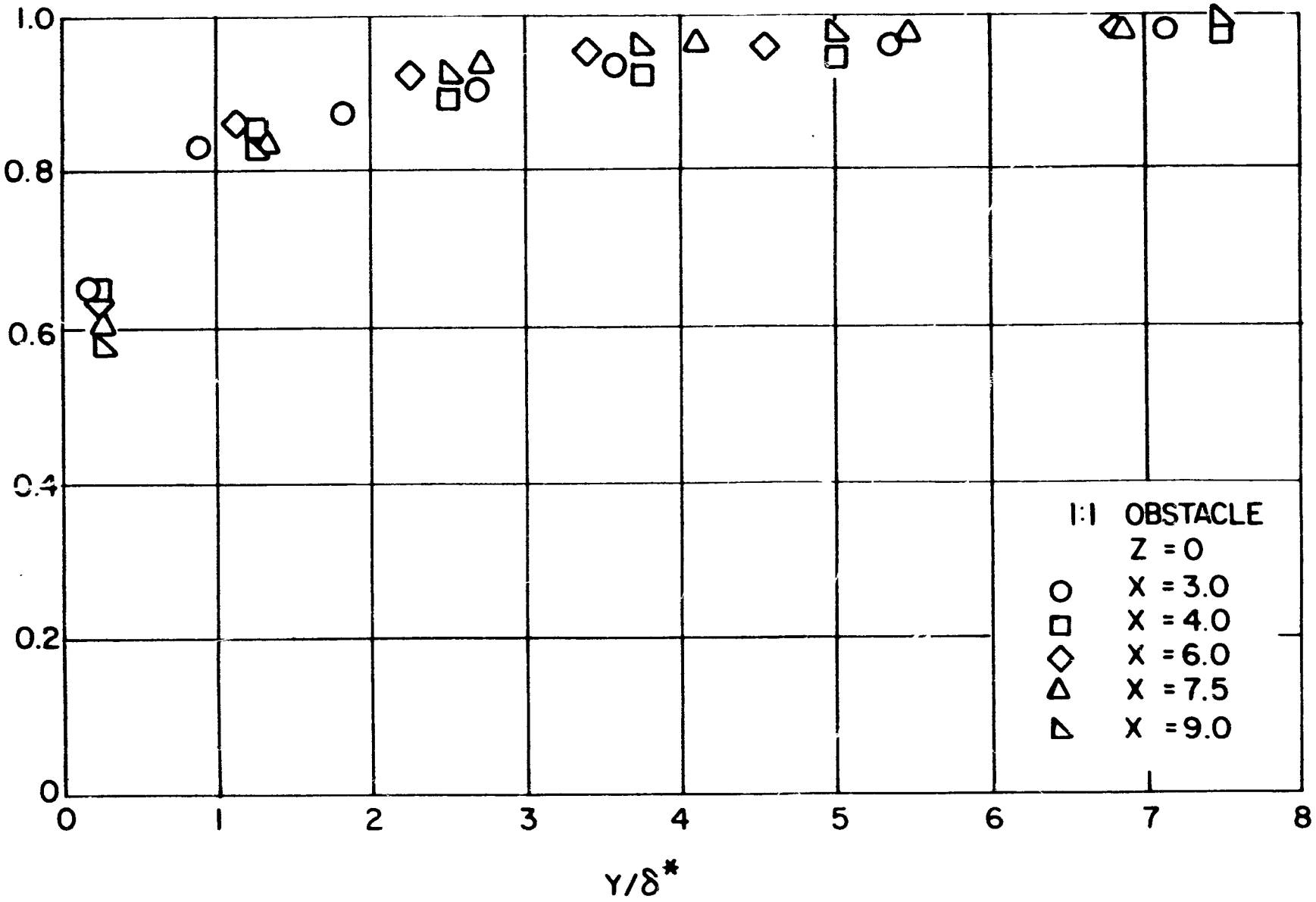

FIG. 14 SIMILARITY PROFILES FOR 1:1 OBSTACLES

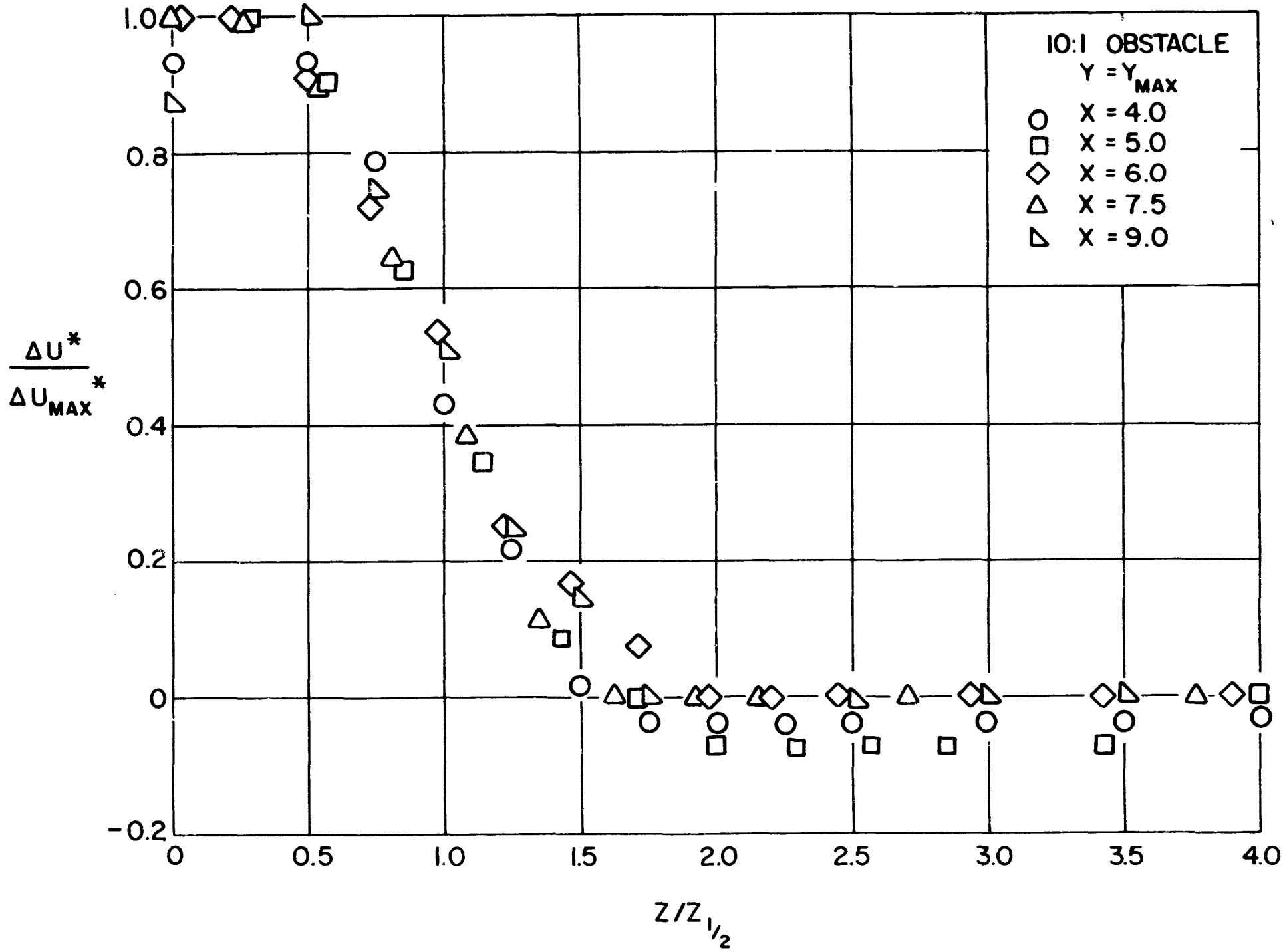

FIG. 15 TRANSVERSE SIMILARITY PROFILES FOR 10:1 OBSTACLE

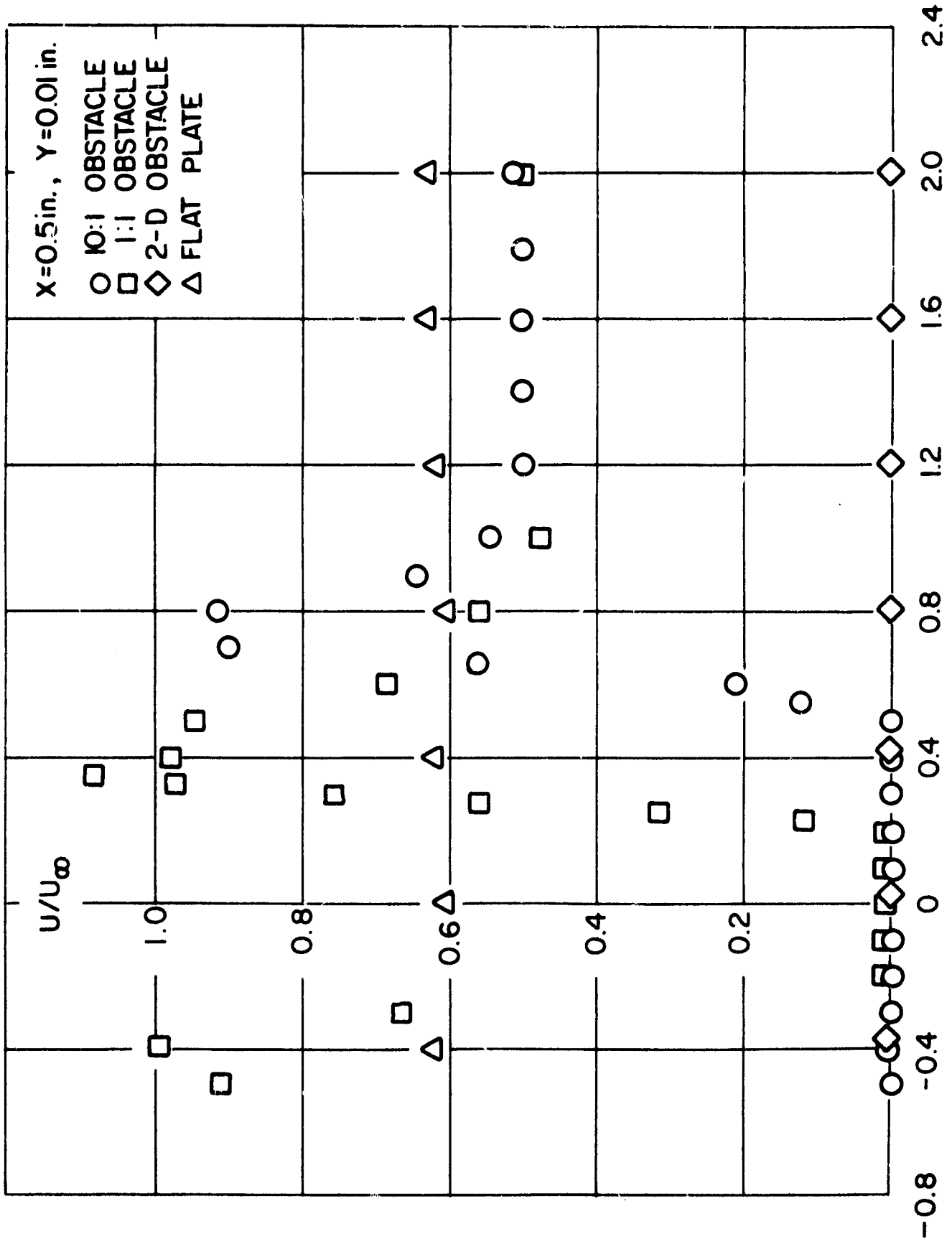

FIG. 16 TRANSVERSE PROFILES X=0.50 IN., Y=0.010 IN.

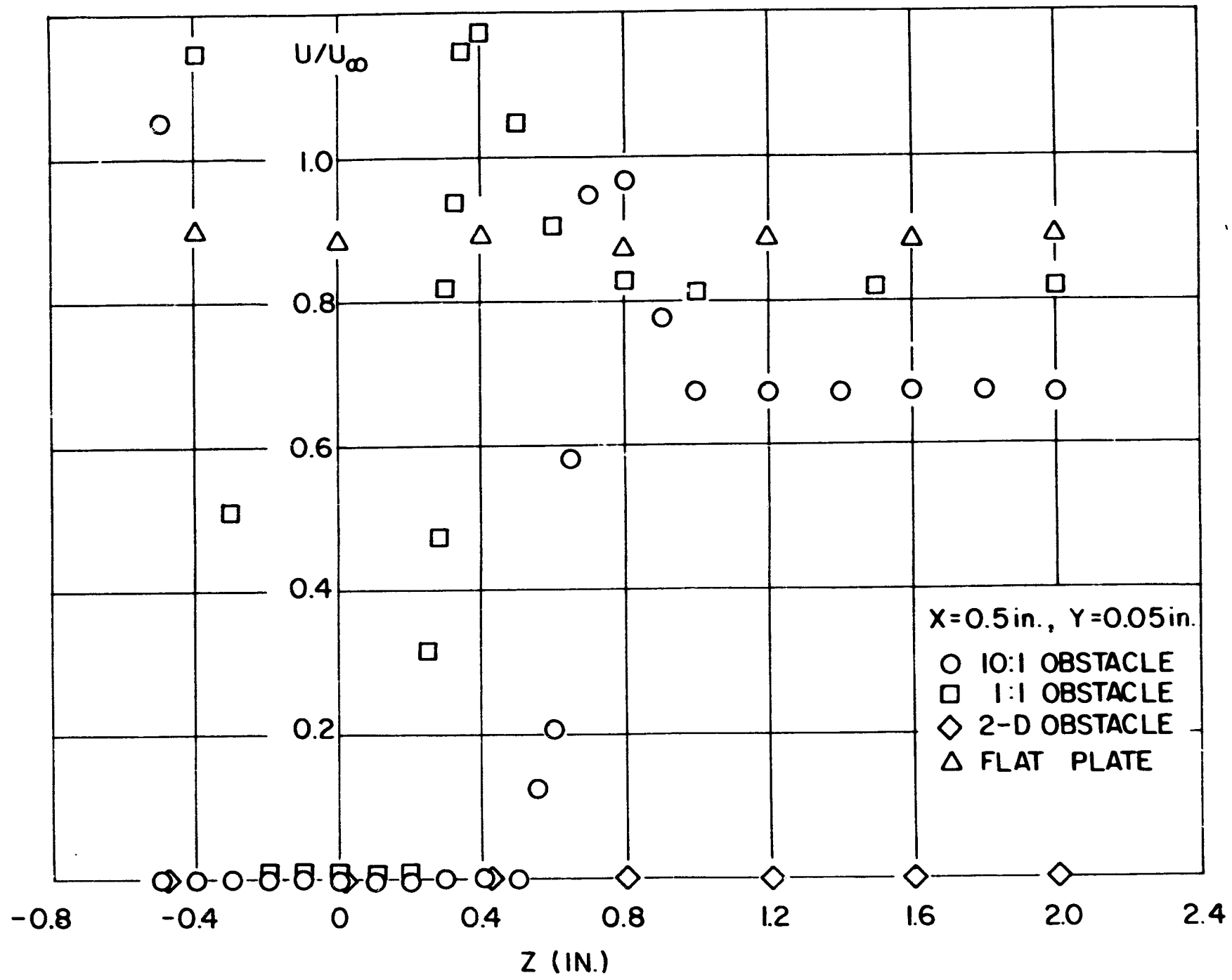

FIG. 17 TRANSVERSE PROFILES X =0.50 IN., Y =0.050 IN.

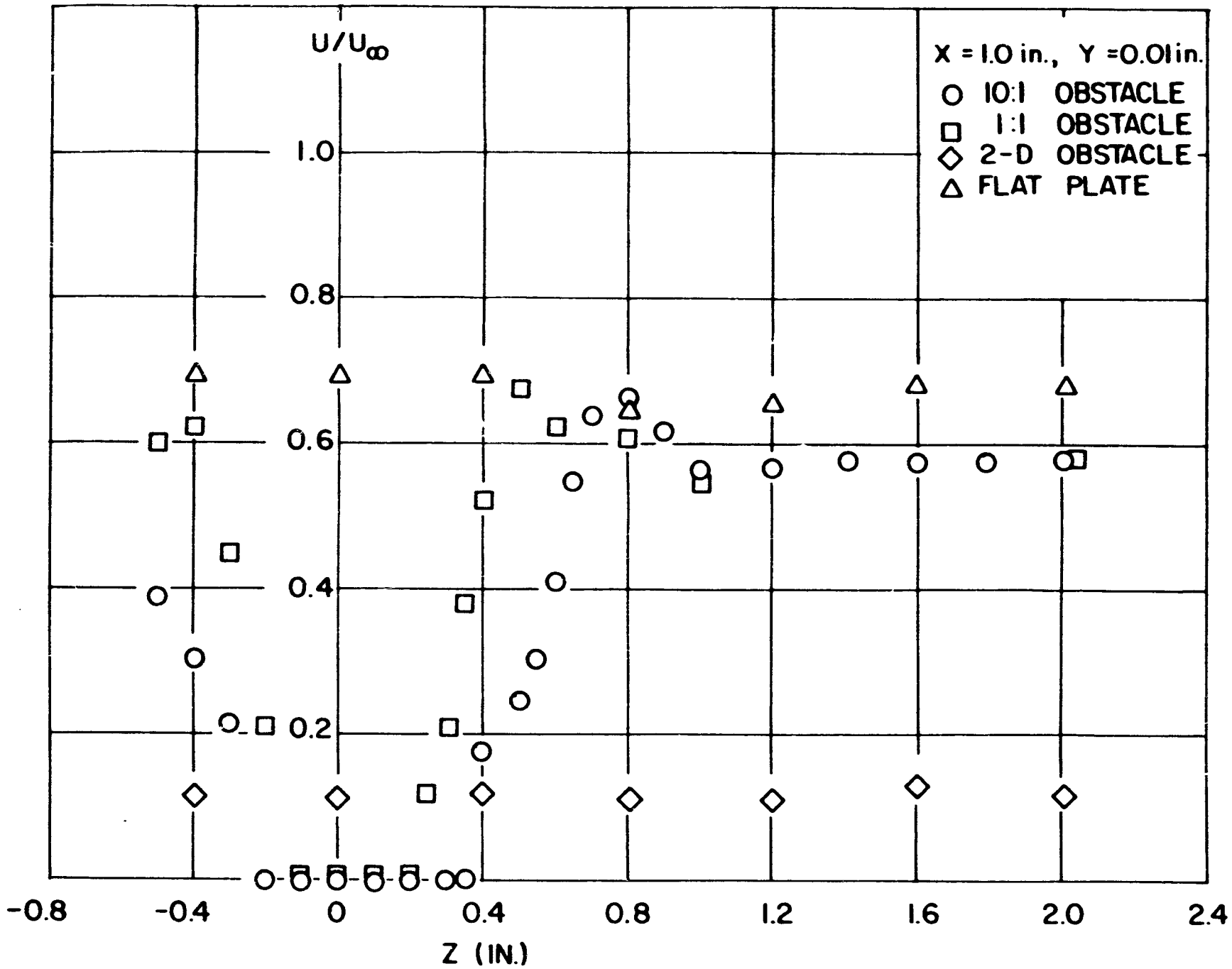

FIG. 18 TRANSVERSE PROFILES X = 1.00 IN., Y = 0.010 IN.

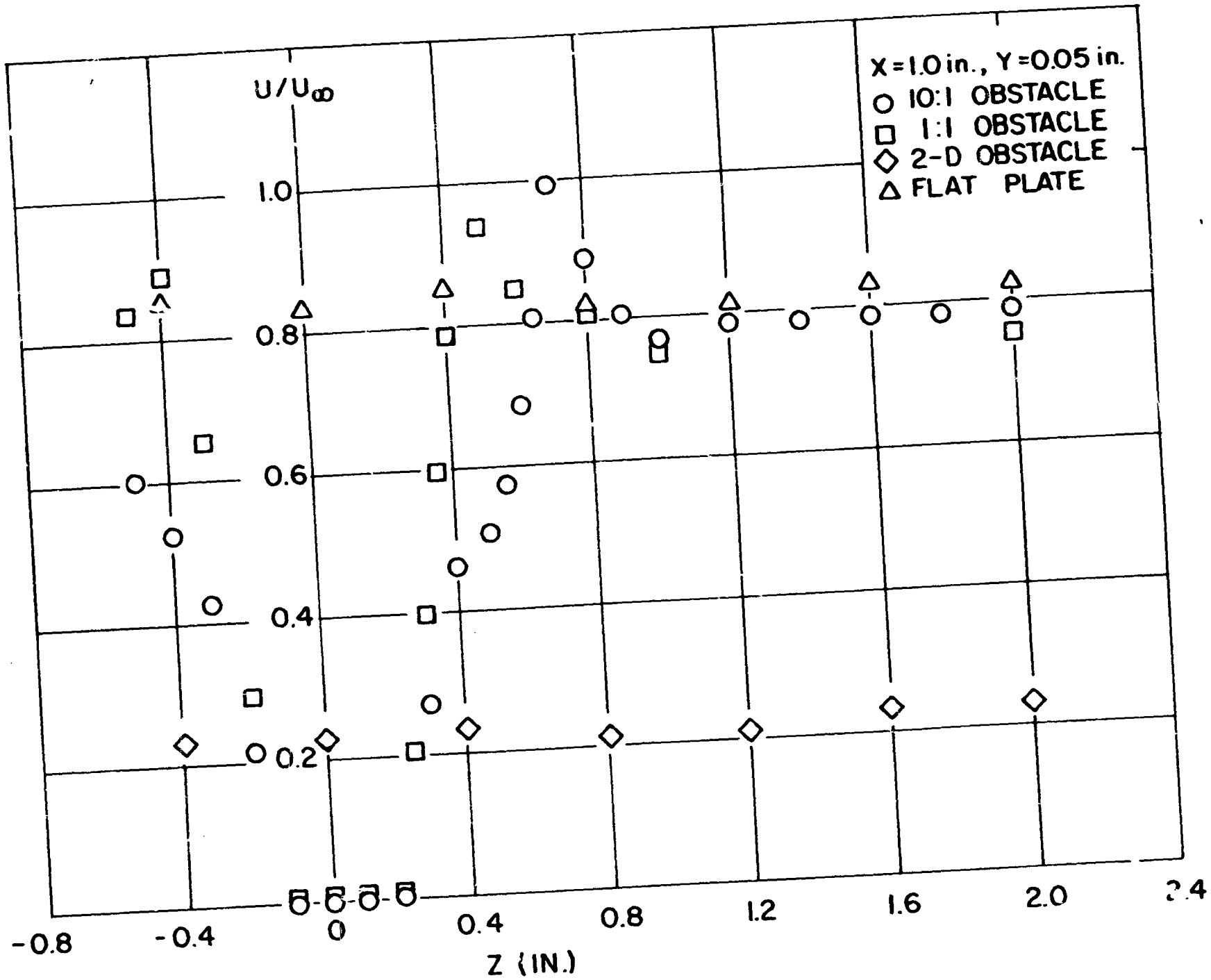

FIG. 19 TRANSVERSE PROFILES X = 1.00 IN., Y = 0.050 IN.

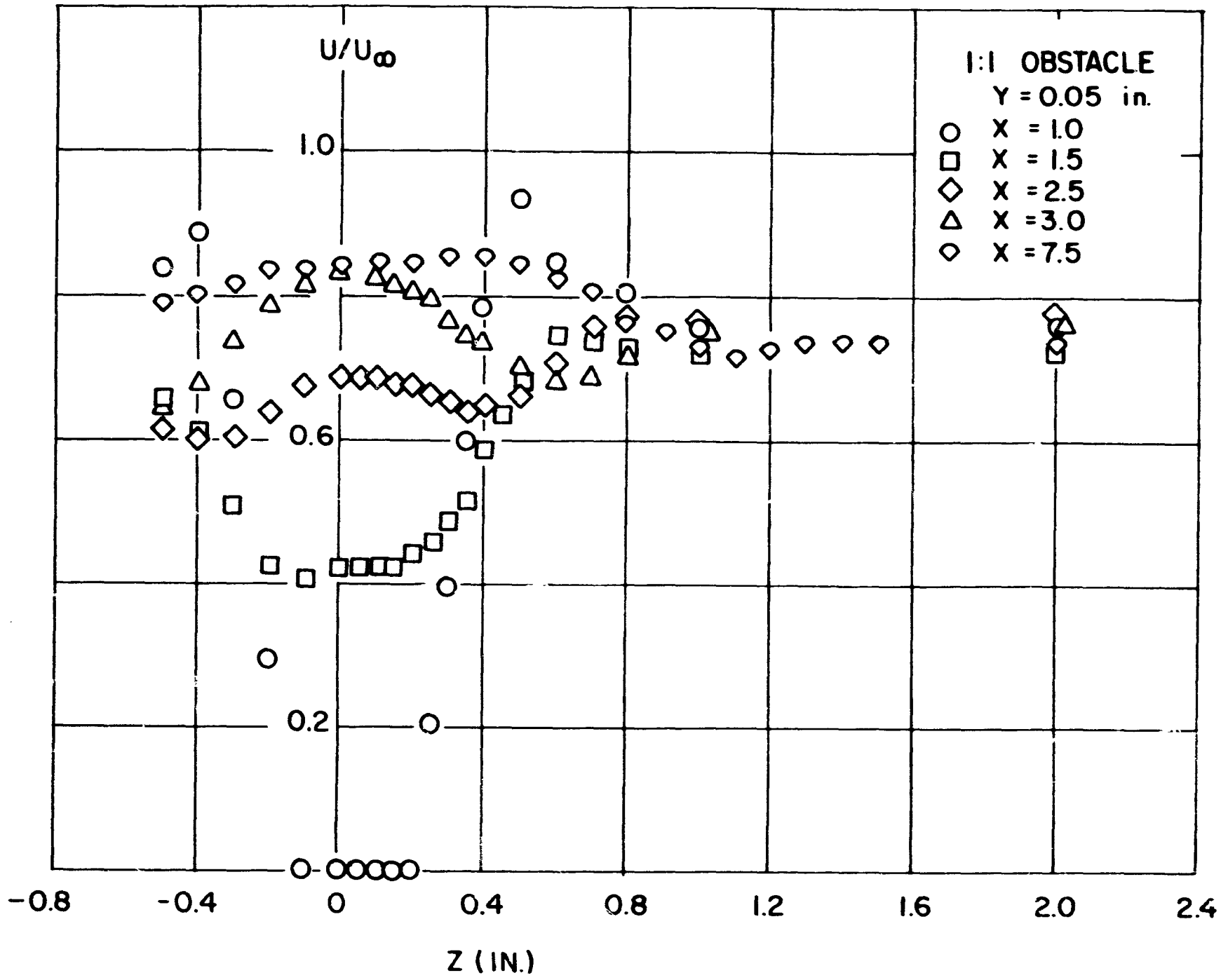

FIG. 20 NON-UNIFORMITY OF TRANSVERSE PROFILES FOR 1:1 OBSTACLE

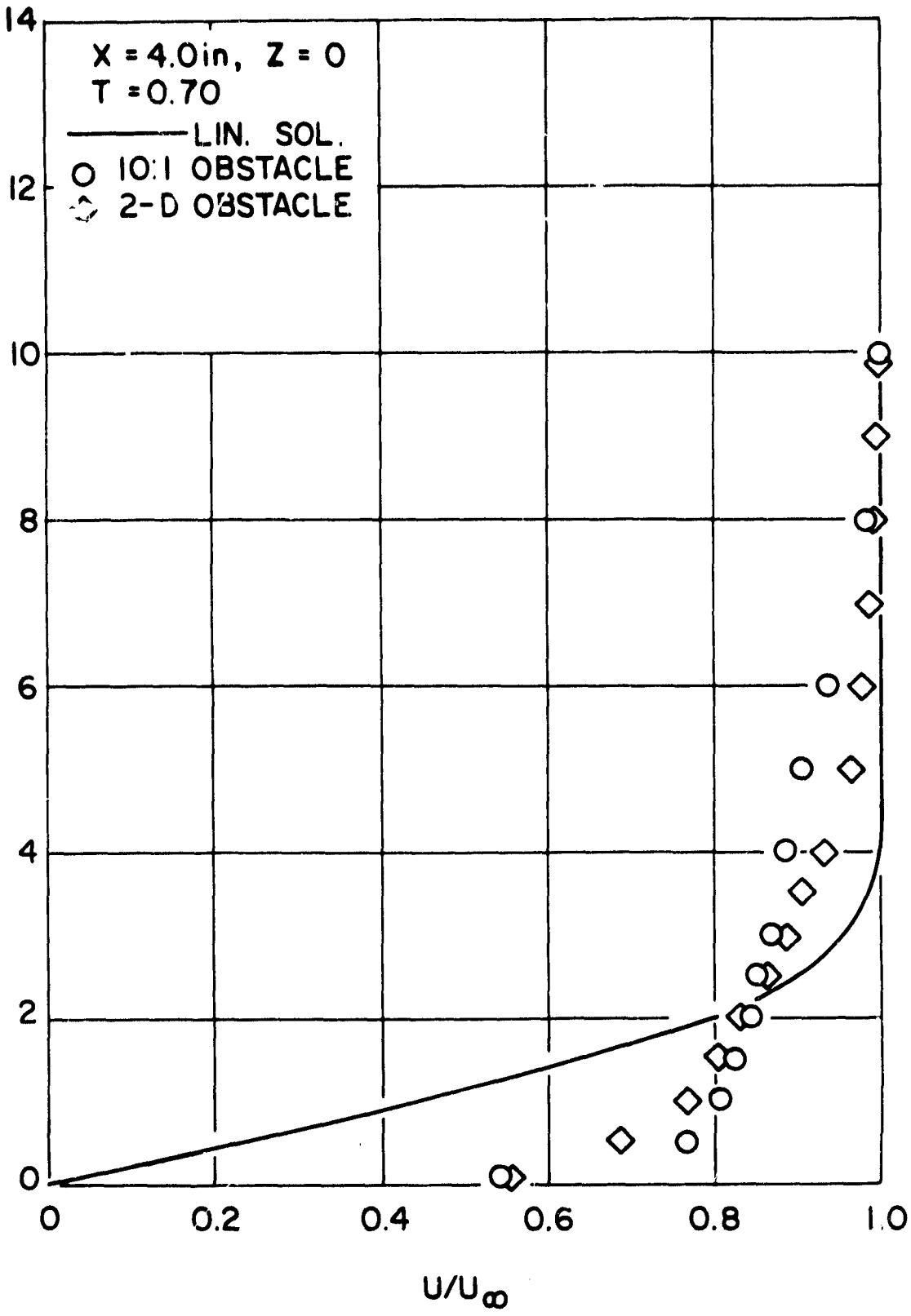

FIG. 21 NORMAL PROFILE AT X=4.0 IN. COMPARED TO LINEARIZED THEORY

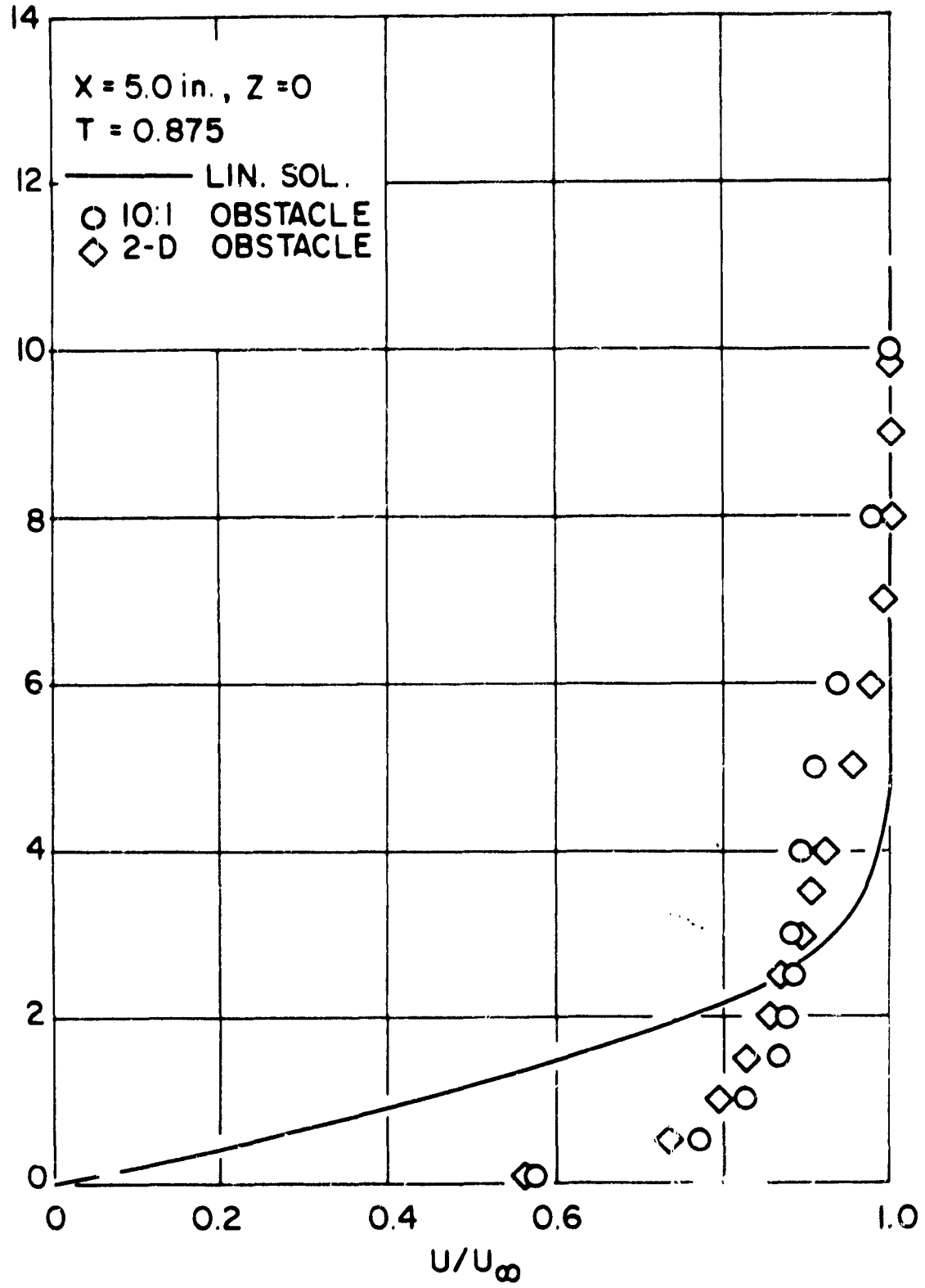

FIG. 22 NORMAL PROFILE AT X = 5.0 IN. COMPARED TO LINEARIZED THEORY

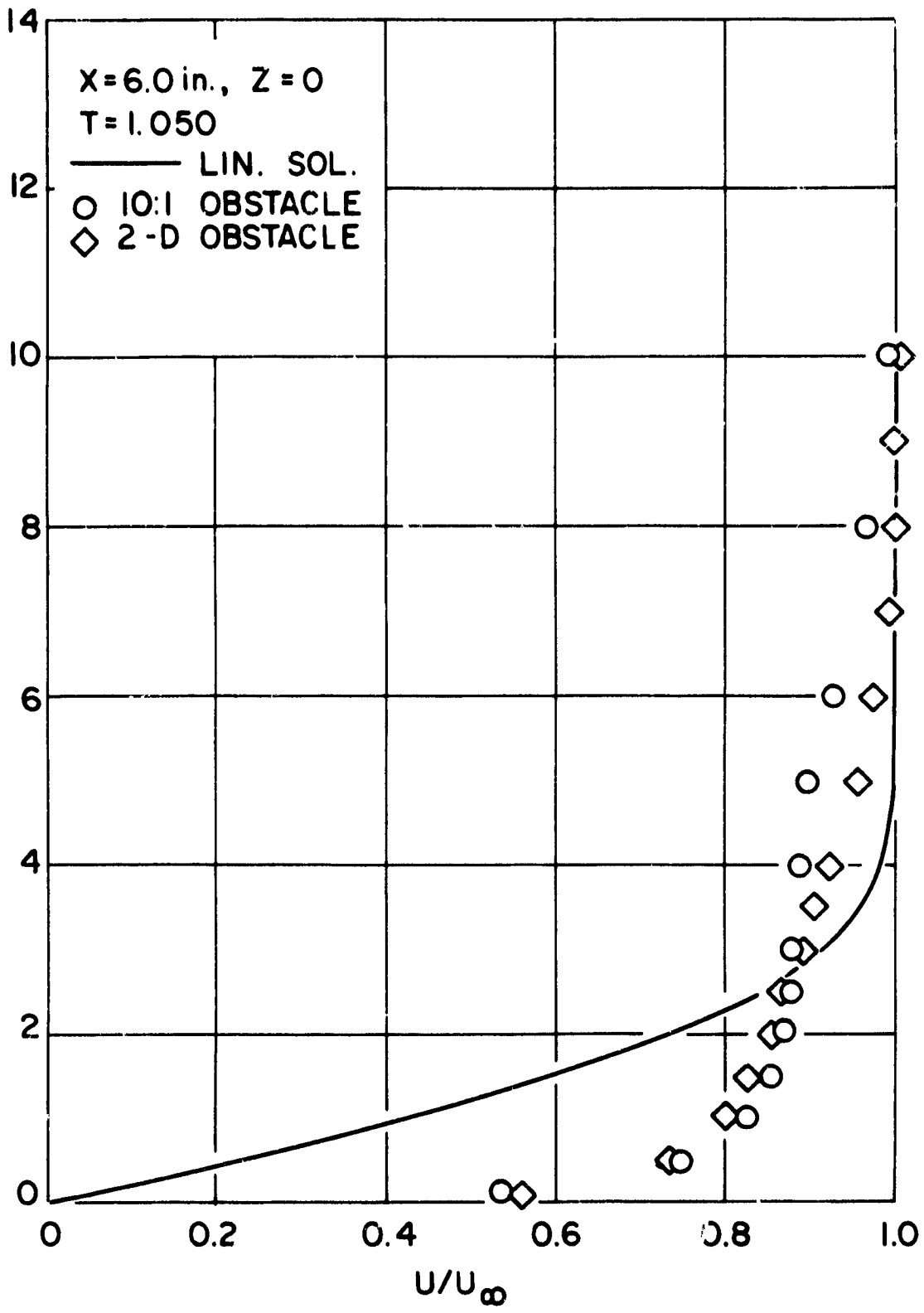

FIG. 23 NORMAL PROFILE AT X=6.0 IN. COMPARED TO LINEARIZED THEORY

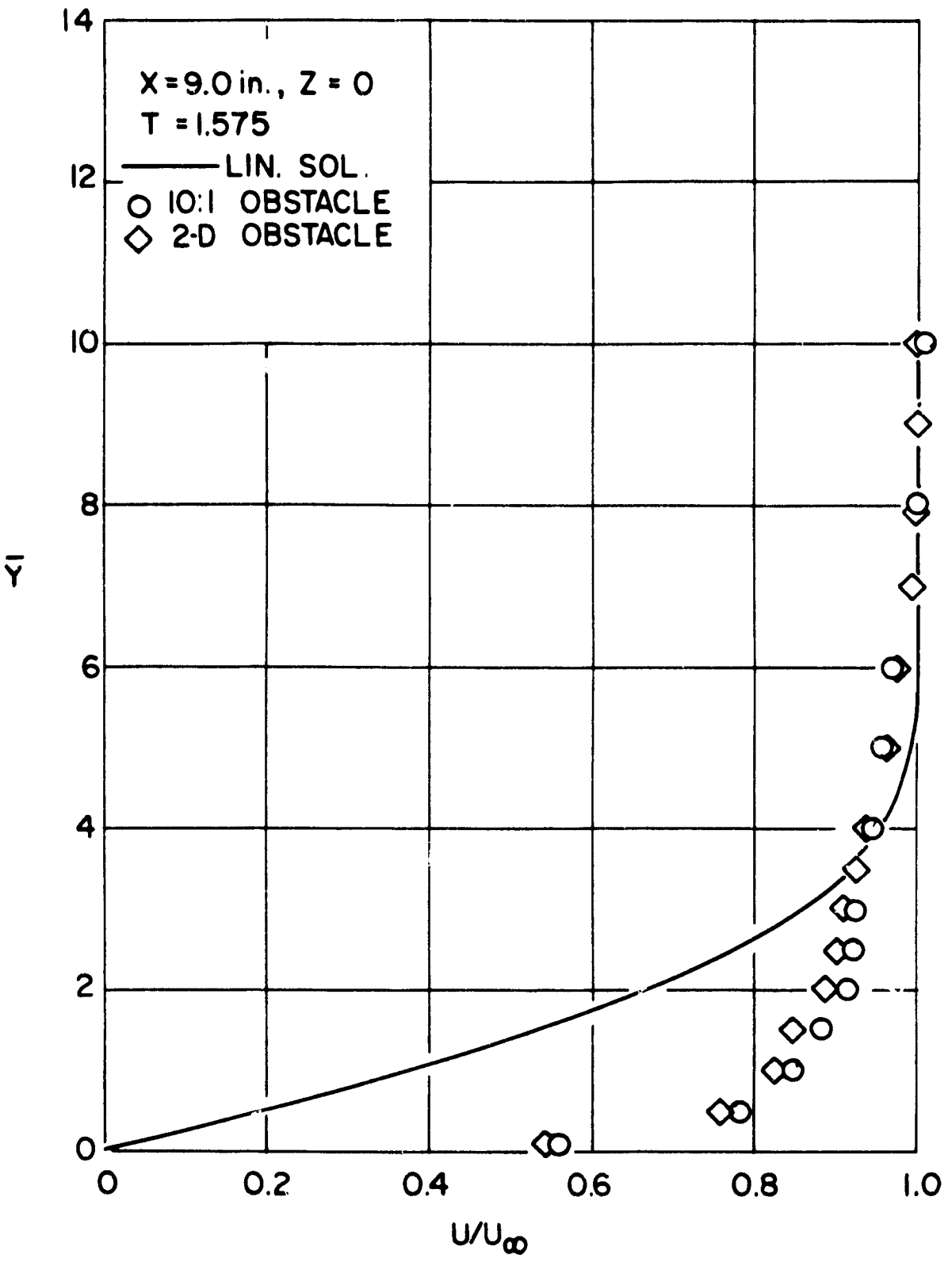

FIG. 24 NORMAL PROFILE AT X = 9.0 IN. COMPARED TO LINEARIZED THEORY

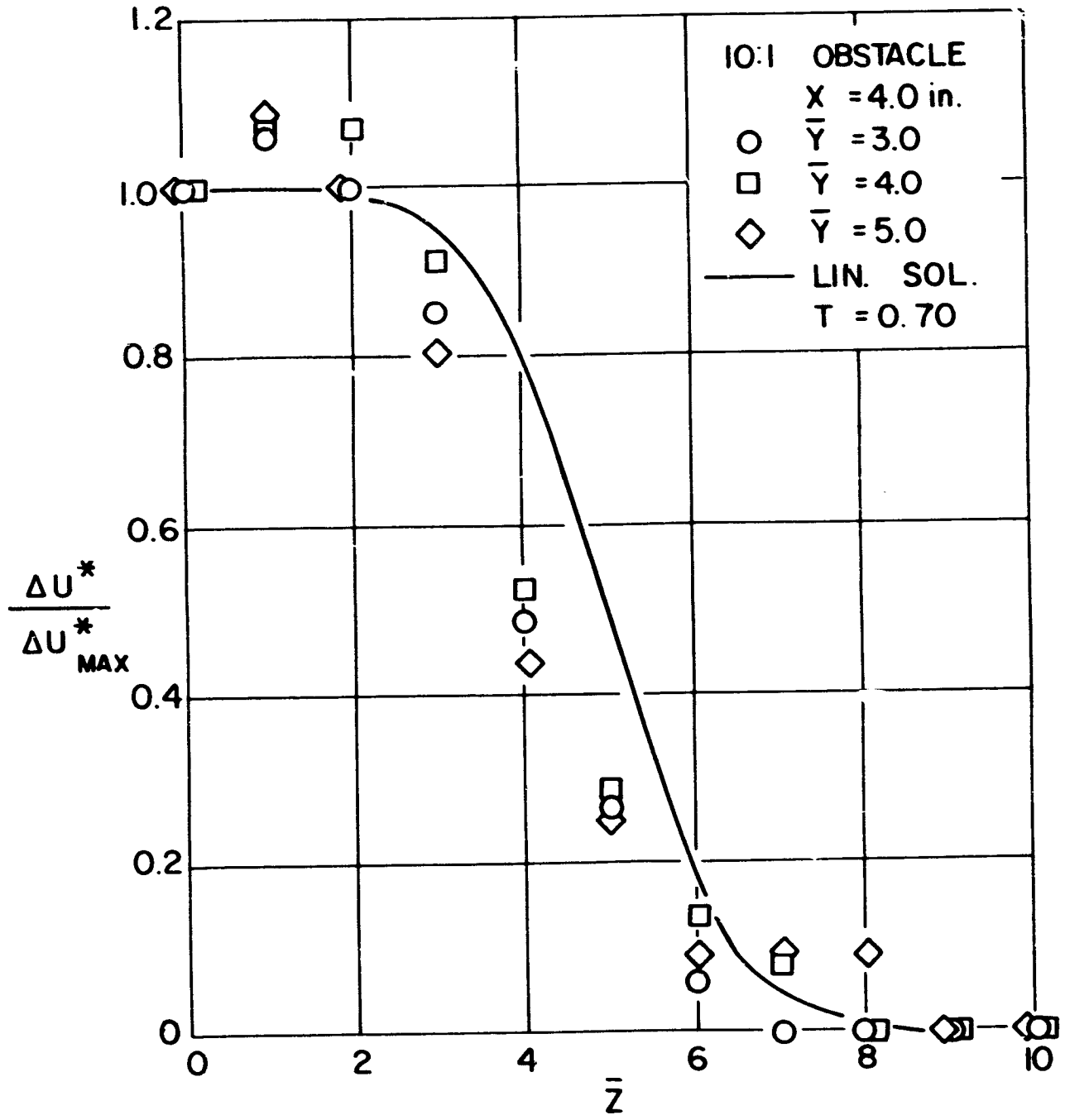

FIG. 25 TRANSVERSE PROFILE AT X = 4.0 IN. COMPARED TO LINEARIZED THEORY

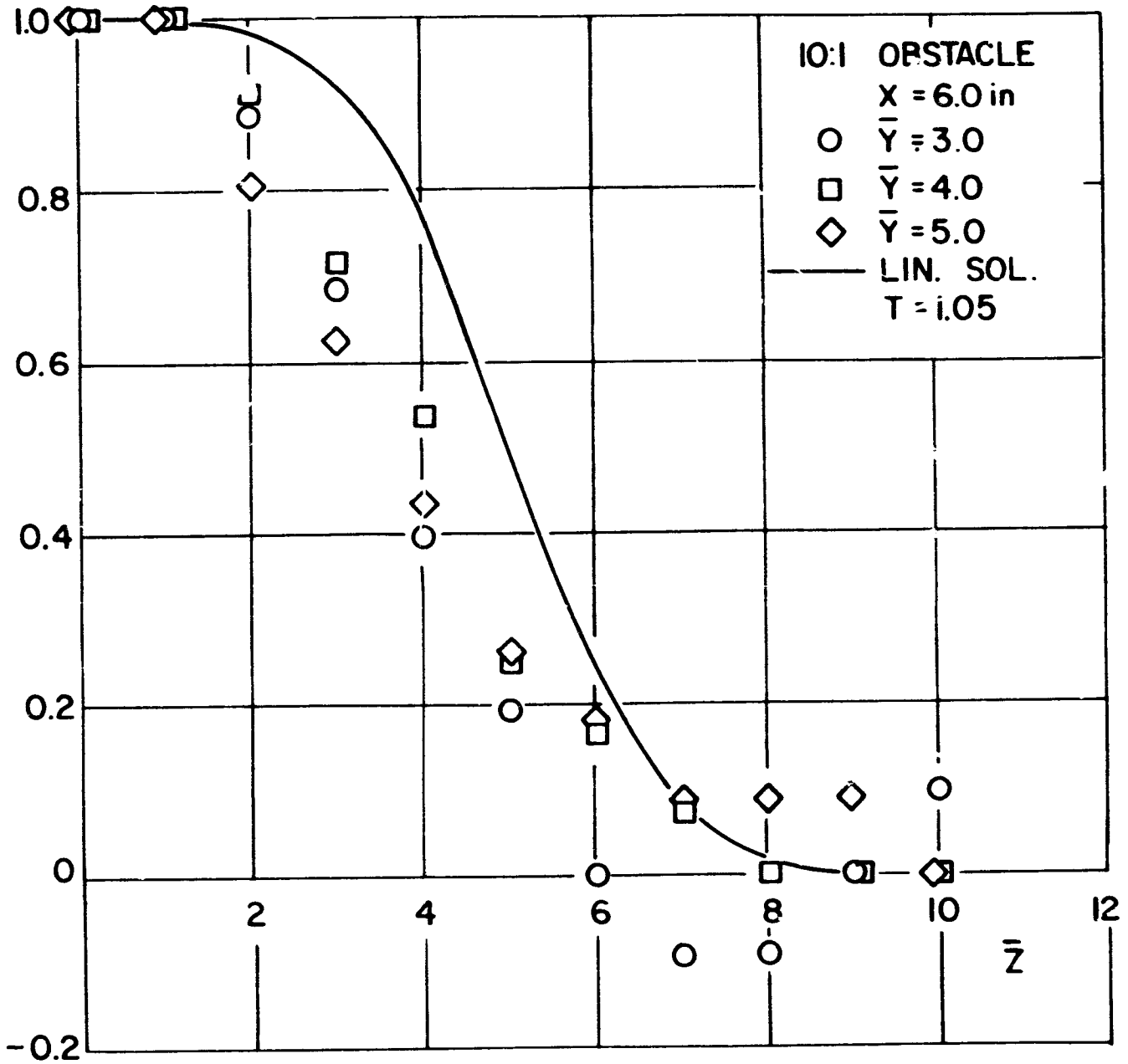

FIG. 26 TRANSVERSE PROFILE AT X = 6.0 IN. COMPARED TO LINEARIZED THEORY

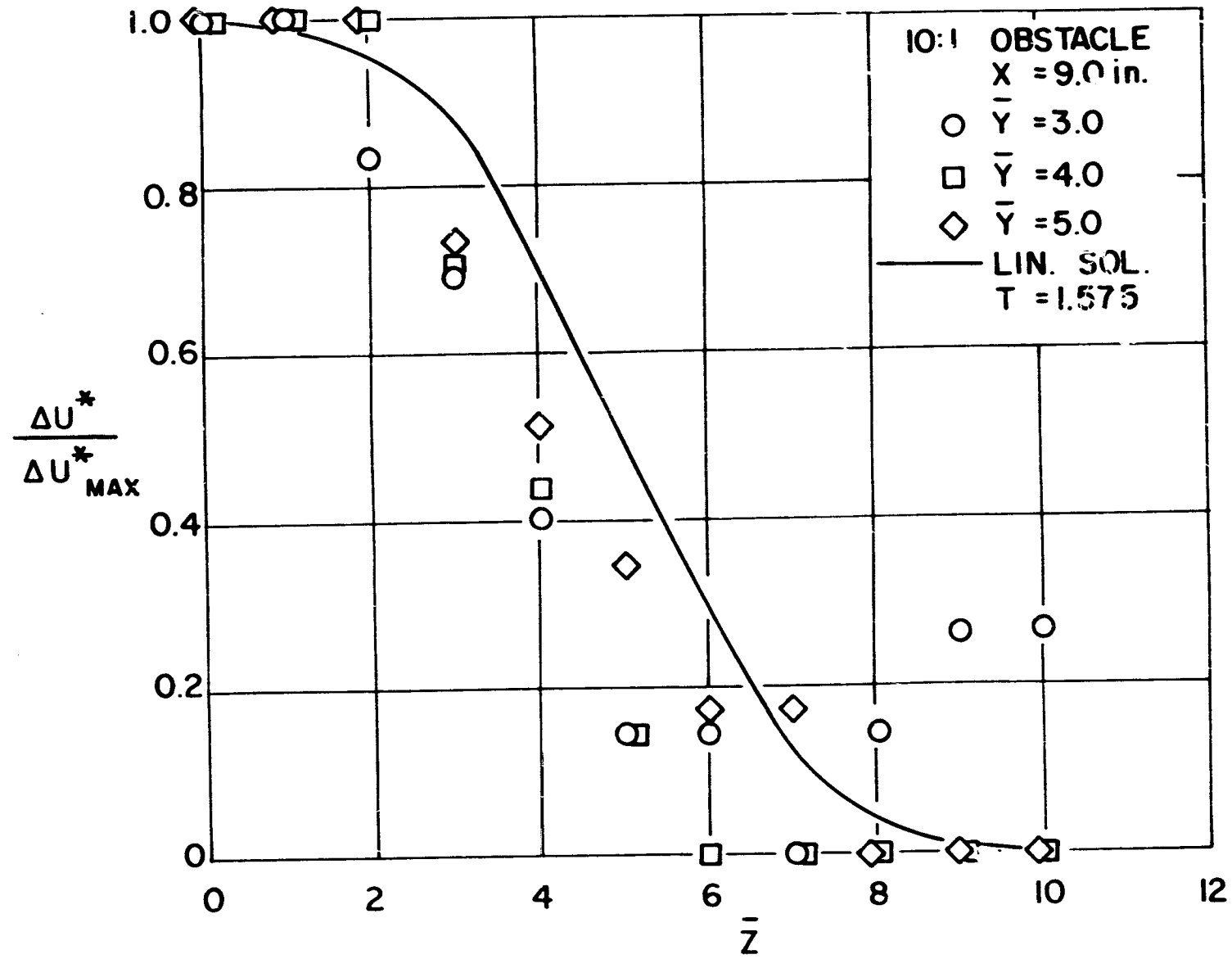

FIG. 27 TRANSVERSE PROFILE AT X = 9.0 IN. COMPARED TO LINEARIZED THEORY

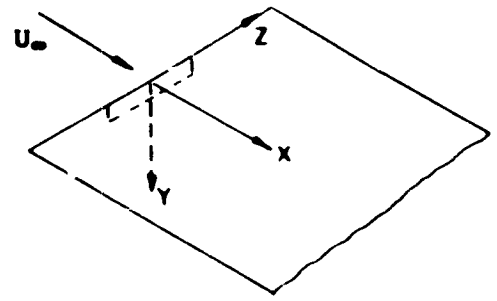

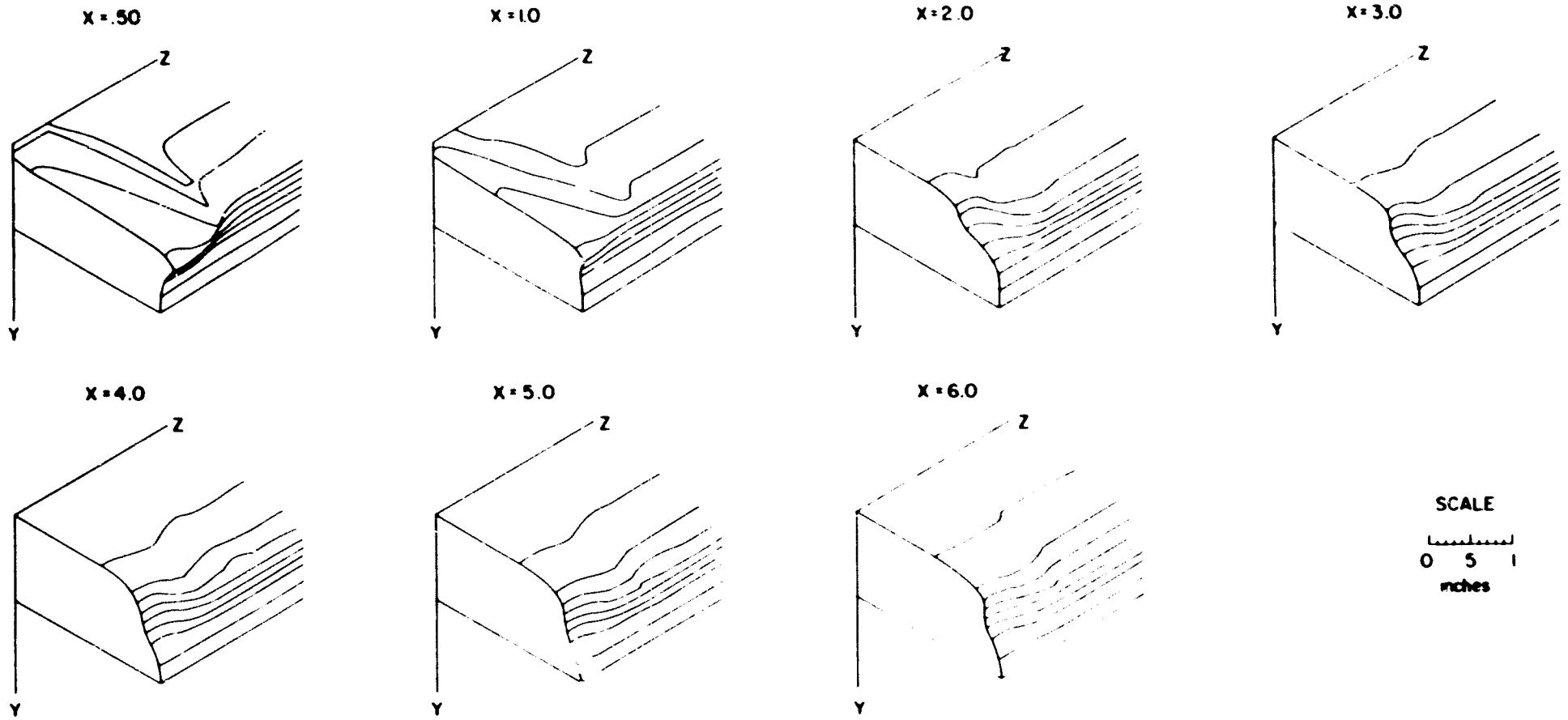

FIG. 28 ISOMETRIC FOR 10:1 OBSTACLE

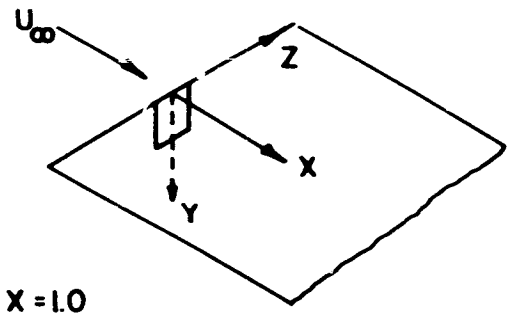

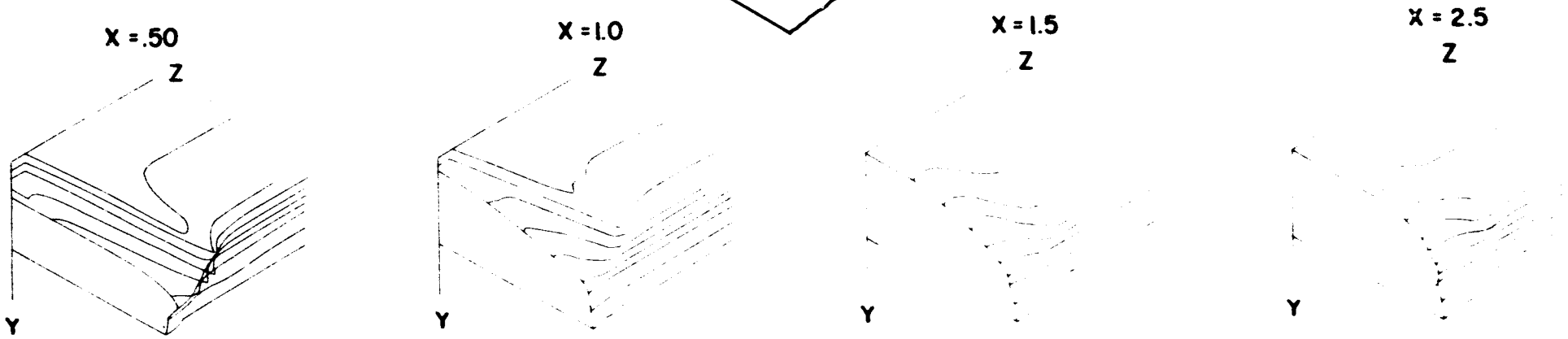

FIG. 29 ISOMETRIC FOR 1:1 OBSTACLE

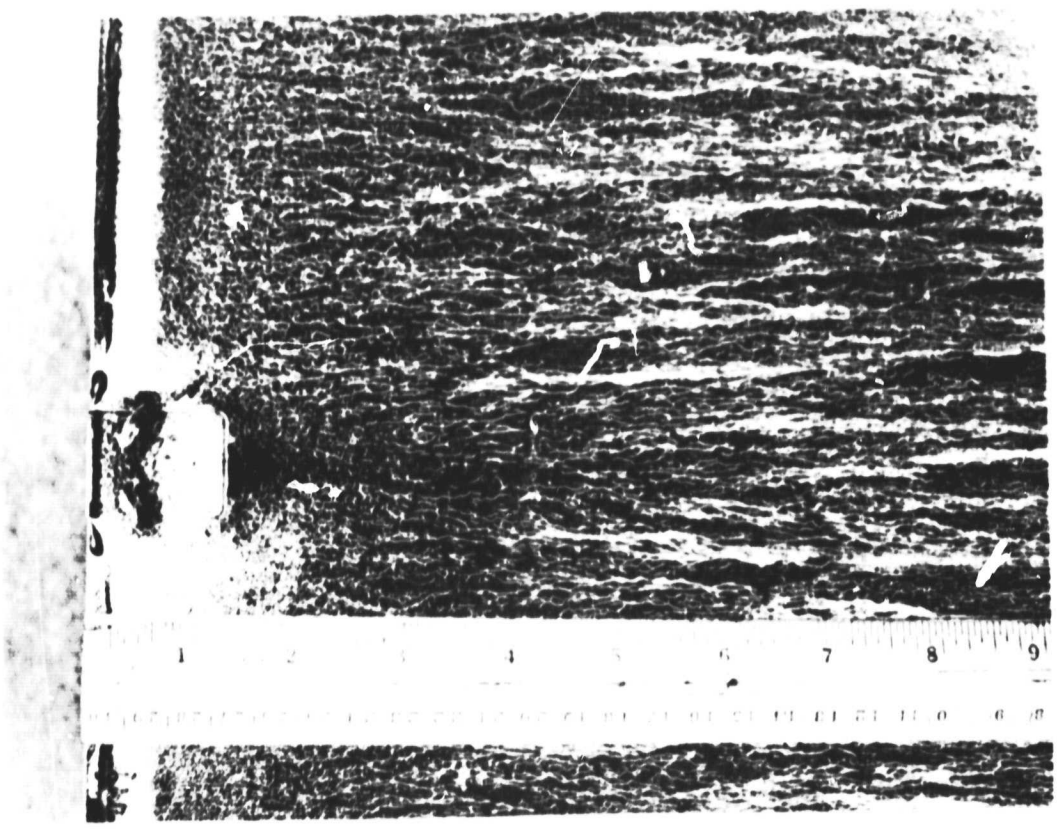

FIG. 30 PHOTO OF FLOW FIELD FOR 10:1 OBSTACLE USING LAMPBLACK

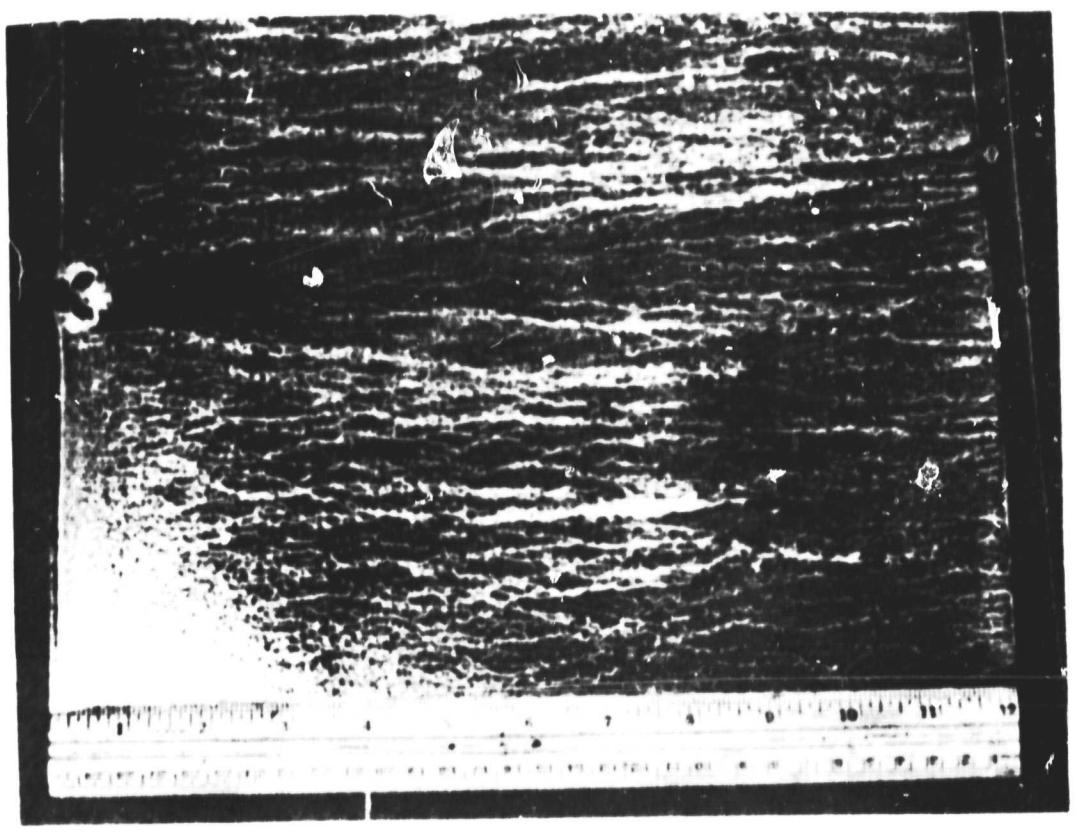

FIG. 31 PHOTO OF FLOW FIELD FOR 1:1 OBSTACLE USING LAMPBLACK

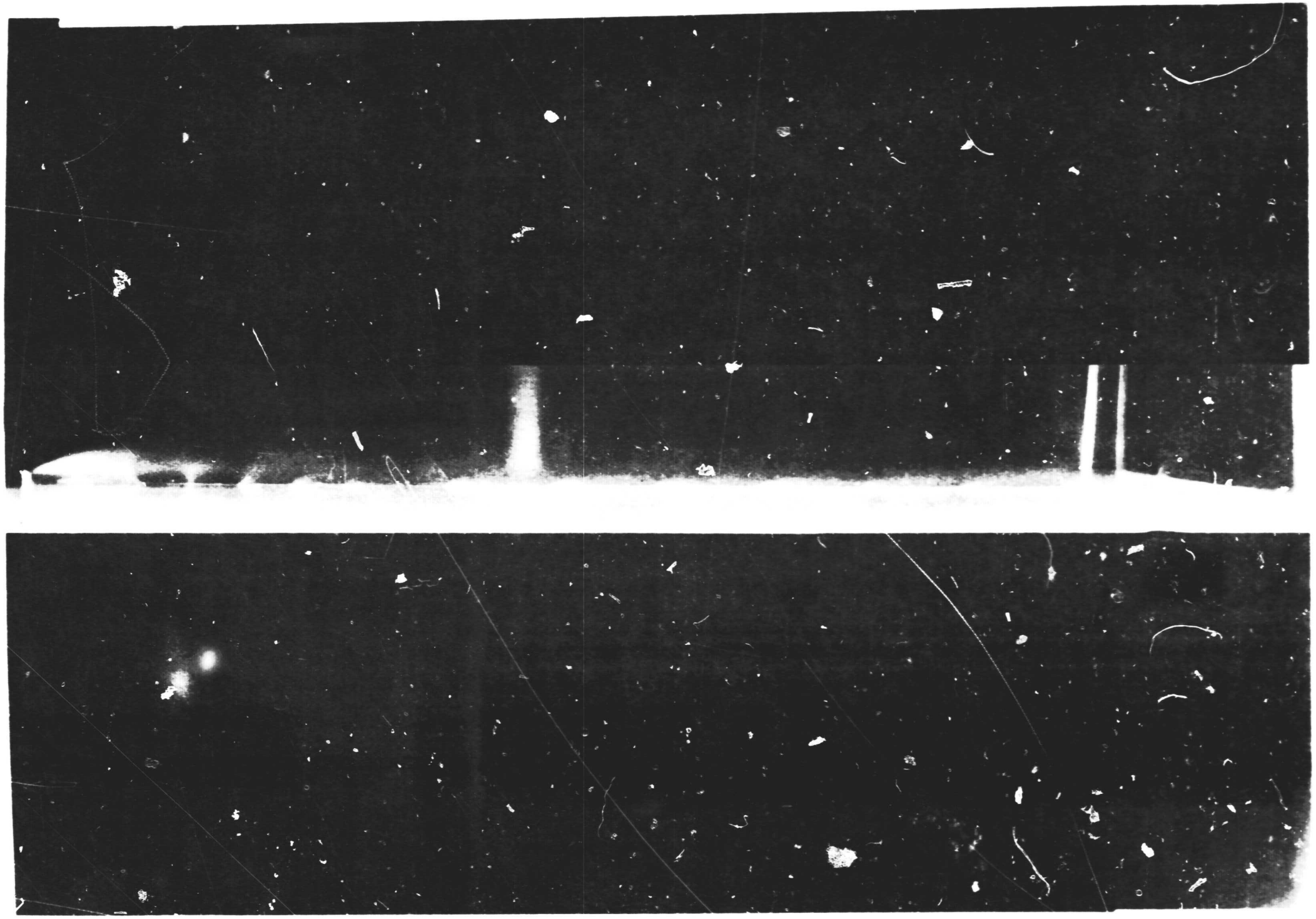

FIG. 32 PHOTO OF FLOW FIELD FOR 10:1 OBSTACLE USING SMOKE

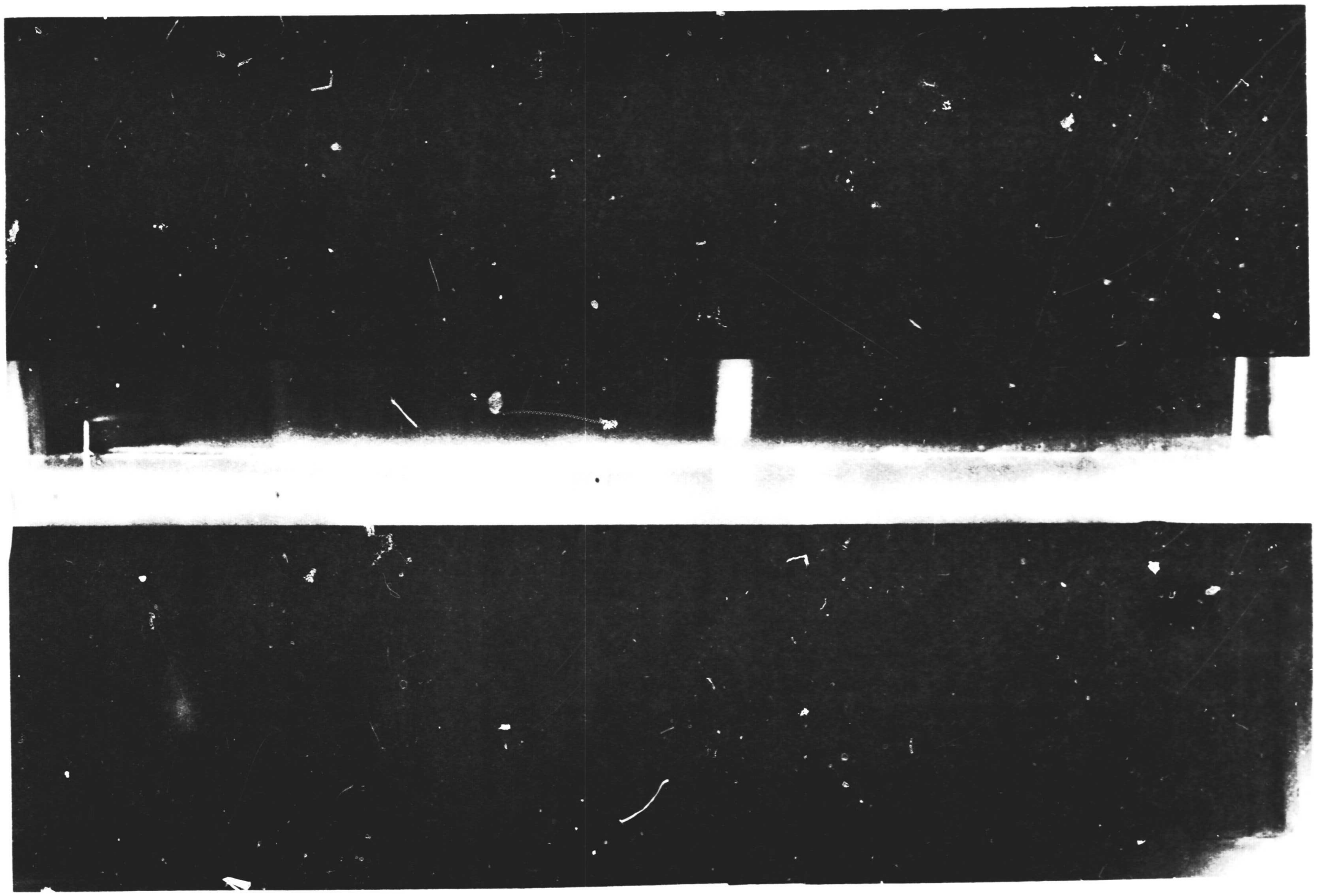

FIG. 33 PHOTO OF FLOW FIELD FOR 1:1 OBSTACLE USING SMOKE